https://doi.org/10.5194/egusphere-2026-3704
Preprint. Discussion started: 10 July 2026


# The Polymorphism of Snow Crystals: Advances in Understanding Vapor-Phase Ice Growth Dynamics via a Tripartite Coupling Framework

Lintao Zhao [1], Jian Liu [1], Yongqing He [1]

[1] Department of Energy and Environment, Southeast University, Nanjing 211189, China

*Correspondence to*: Jian Liu (liujian8@seu.edu.cn); Yongqing He (yqhe@seu.edu.cn)

**Abstract.** Vapor-phase growth of snow crystals generates a striking diversity of morphologies—from simple faceted prisms to complex stellar dendrites, hollow columns, bullet rosettes, and rare trigonal forms—from a single hexagonal ice Ih lattice. This polymorphism emerges from the interplay between temperature-dependent anisotropy in facet-specific attachment kinetics, diffusion-limited vapor transport, and morphological instabilities at the ice–vapor interface. Despite extensive research, no first-principles predictive framework exists; existing models depend on empirical parameterizations of the attachment coefficient $\alpha(T)$ and provide limited insight into how trace atmospheric impurities alter step energetics, quasi-liquid layer (QLL) stability, and growth kinetics. Here we review two decades of advances in laboratory experiments, theory, and simulations since Libbrecht's 2005 synthesis. We introduce a tripartite coupling framework that unifies the ice crystal, water vapor, and background atmospheric constituents (including impurities). Central to the framework is the Structure-Dependent Attachment Kinetics (SDAK) model, which accounts for habit transitions, edge-sharpening instabilities, trigonal symmetry breaking, and QLL-mediated step dynamics. We discuss extensions to climate microphysics, icephobic surface design, and planetary cryoscience, and identify key remaining challenges and future directions.

**Keywords**: vapor-phase ice growth, snow crystal polymorphism, ice-vapor interface, facet-specific attachment kinetics, quasi-liquid layer (QLL), Structure-Dependent Attachment Kinetics (SDAK) model.

## 1. Introduction

The vapor-phase growth of snow crystals produces diverse morphologies from a single hexagonal ice Ih lattice through the coupling of molecular-scale interfacial processes and macroscopic diffusion fields (Petrenko and Whitworth, 1999; Libbrecht, 2005). Snow crystals exhibit pronounced polymorphism, ranging from simple faceted prisms to thin plates, stellar dendrites, columns, hollow columns, bullet rosettes, and rare trigonal forms. This diversity arises from diffusion-limited vapor transport, facet-specific attachment kinetics, and morphological instabilities, establishing snow crystals as a model system for studying faceting, branching, and pattern formation in non-equilibrium solidification (Langer, 1980; Libbrecht, 2005; Libbrecht and Walkling, 2023).

https://doi.org/10.5194/egusphere-2026-3704
Preprint. Discussion started: 10 July 2026


These mechanisms inform atmospheric processes including cloud formation, precipitation, and climate modeling, and extend to materials applications such as icephobic surfaces and snow management on infrastructure (Cao et al., 2009; Morrison et al., 2020; Vázquez-Martín et al., 2021; Chu et al., 2024). Analogous vapor-phase deposition on icy moons (Europa and Enceladus) under low-pressure, low-temperature conditions (<100 K) may generate distinctive ice structures linked to subsurface oceans and cryovolcanism, with implications for planetary science and astrobiology (Porco et al., 2006; Roth et al., 2014; Postberg et al., 2018).

Despite decades of study, no comprehensive first-principles framework exists for predicting snow crystal polymorphism. Three core challenges remain. First, trace atmospheric impurities—organics, salts, and mineral dust—can shift habit-transition temperatures by several degrees Celsius via effects on step energies, QLL dynamics, and attachment coefficients, yet the underlying molecular mechanisms and their quantitative incorporation into models remain largely unexplored. Second, $\alpha(T)$ parameterizations rely on empirical fits to laboratory data rather than derivations from interfacial physics, restricting predictive power for rare morphologies or extreme conditions. Third, multi-scale modeling under realistic atmospheric dynamics—incorporating variable temperature, humidity, sedimentation, ventilation, and aggregation—remains nascent, hindering accurate forecasts of habit-dependent cloud microphysics, radiative transfer, and climate effects.

Recent advances from high-precision diffusion-chamber experiments (Libbrecht and Morrison, 2008; Libbrecht, 2011a), atomistic simulations (Barrett et al., 2012; Hong et al., 2024), and in-situ atmospheric observations (Bailey and Hallett, 2009) have shifted the field from qualitative descriptions toward quantitative, mechanistic understanding of anisotropic growth and symmetry breaking (Libbrecht, 2005, 2017). Key progress includes precise measurements of facet-specific growth rates that define temperature-dependent attachment kinetics (Libbrecht, 2011a), molecular dynamics simulations that reveal the regulatory role of quasi-liquid layers (QLLs) in step energetics and propagation (Hong et al., 2024), and refined attachment-coefficient parameterizations across environmental conditions (Libbrecht and Arnold, 2009a; Yokoyama et al., 2011; Libbrecht and Rickerby, 2013; Libbrecht, 2016).

Building on Libbrecht's influential 2005 overview (Libbrecht, 2005), this review synthesizes two decades of experimental, theoretical, and computational progress in snow crystal growth. It moves beyond single-factor and phenomenological treatments by developing a tripartite coupling framework that integrates the ice crystal, water vapor, and atmospheric constituents to account for the multi-parameter control of morphology. We also connect these physical insights to applications in climate modeling, anti-icing engineering, and planetary ice science.

We synthesize recent advances, critically assess limitations of existing models, highlight unresolved challenges, and outline directions for future research. The scope is limited to atmospheric vapor-phase growth of ice Ih, excluding liquid-phase freezing, high-pressure polymorphs, and post-depositional metamorphism.

https://doi.org/10.5194/egusphere-2026-3704
Preprint. Discussion started: 10 July 2026


## 2. Physical Processes of Snow Crystal Formation via Tripartite Coupling Mechanism

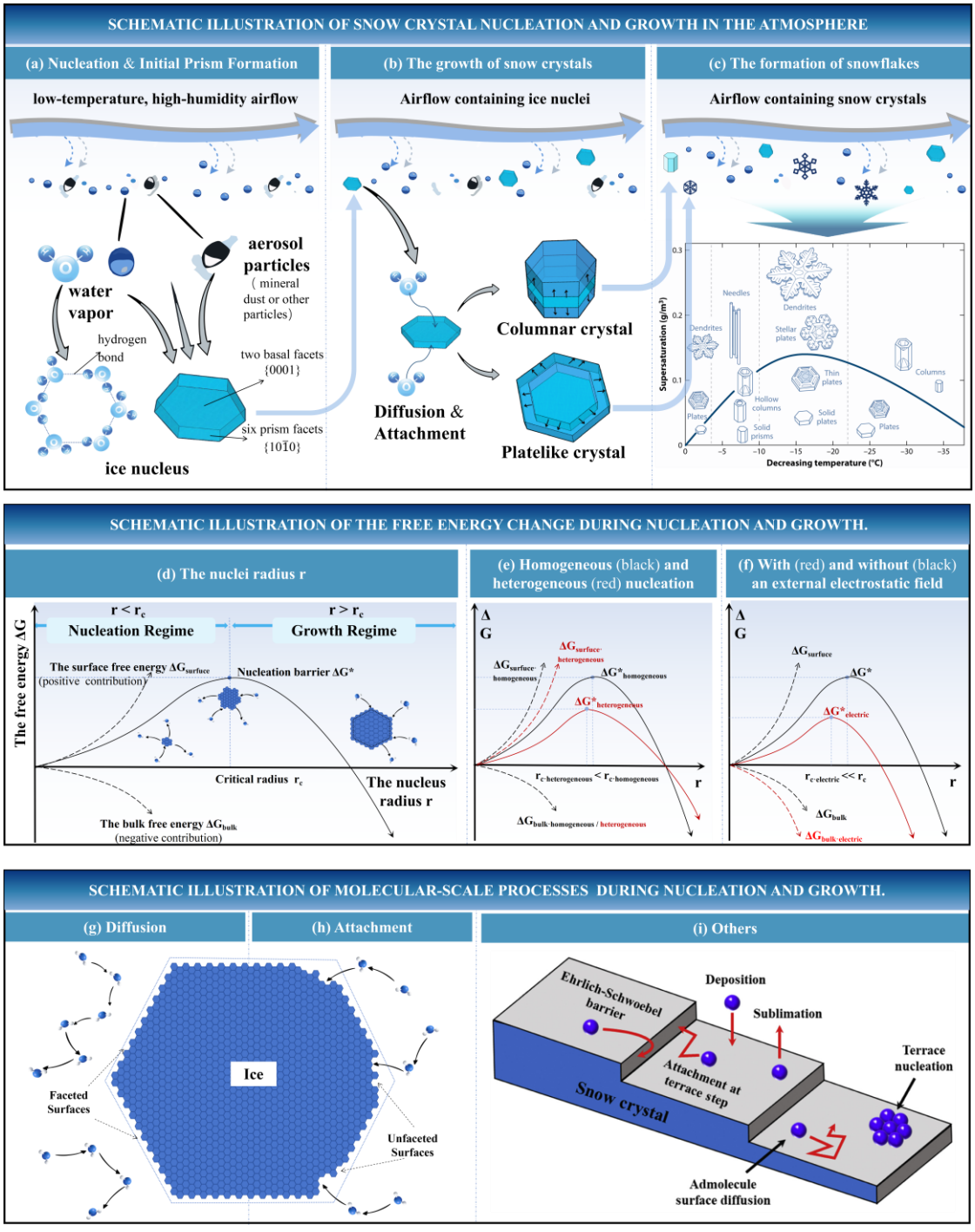


**Figure 1: Multi-scale schematic of the tripartite coupling mechanism in atmospheric snow crystal formation, integrating macroscopic growth stages, molecular-scale interfacial processes at the ice–vapor interface, and nucleation thermodynamics.**

https://doi.org/10.5194/egusphere-2026-3704
Preprint. Discussion started: 10 July 2026


**(a)–(c) Macroscopic stages: (a) nucleation and initial hexagonal prism formation in low-temperature supersaturated airflow; (b) sustained crystal growth driven by diffusion–attachment coupling; (c) morphological evolution into snow crystals (inset: Nakaya habit diagram depicting temperature- and supersaturation-dependent polymorphism). (d)–(f) Free-energy changes of nucleation: (d) free-energy change $\Delta G$ as a function of nucleus radius r (nucleation regime for $r < r_c$ and growth regime for $r > r_c$); (e) homogeneous versus heterogeneous (red) nucleation barriers; (f) reduction of the nucleation barrier by an external electrostatic field (red). (g)–(i) Molecular-scale processes at the ice–vapor interface: (g) vapor diffusion to the ice surface; (h) molecular attachment kinetics; (i) surface dynamics including the Ehrlich–Schwoebel barrier, step attachment, admolecule surface diffusion, terrace nucleation, deposition, and sublimation.**

Snow crystal formation and evolution in the atmosphere exemplify a cross-scale, non-equilibrium interfacial process in which molecular events at the ice–vapor interface couple to macroscopic diffusion fields. As shown in Fig. 1, development proceeds through three stages: (1) nucleation and formation of an initial faceted prism that templates all subsequent growth (Fig. 1a) (Kärcher, 2020; Huang et al., 2021); (2) sustained growth governed by the coupling of vapor diffusion and facet-specific attachment kinetics (Fig. 1b) (Libbrecht and Arnold, 2009a; Pedersen et al., 2014; Libbrecht, 2019a; Hoffmann, 2020; Schlesinger et al., 2020; Hauer et al., 2021); and (3) morphological evolution driven by anisotropic competition between basal and prism facets together with amplification of instabilities (Fig. 1c) (Libbrecht and Arnold, 2009b; Libbrecht, 2011b; Libbrecht, 2019a).

Beyond the macroscale growth pathway, Fig. 1 also integrates the free-energy landscape of nucleation (panels d–f) and molecular-scale interfacial processes (panels g–i) (Zhang et al., 2012; Murray et al., 2012). This integrated multiscale visualization provides a clear mechanistic framework for the detailed interfacial analysis in the upcoming subsections.

### 2.1 From Nucleation to Initial Prism Formation

Ice nucleation is the crucial first step in vapor-phase snow crystal formation, linking supersaturated vapor with the development of a solid ice embryo at the ice–vapor interface. Under typical tropospheric conditions, heterogeneous nucleation predominates, with aerosol particles such as mineral dust, biological fragments, or combustion-derived nuclei acting as ice-nucleating particles that lower the energy barrier at the interface by providing an organized template for molecular alignment (Zhang et al., 2012). This process allows nucleation over a wide temperature range (roughly -6°C to -40°C), with the exact range depending on the aerosol's nucleating efficiency and surface chemistry. Conversely, homogeneous nucleation within pure water droplets requires extreme supercooling (close to -40°C) and occurs much less often in natural clouds due to the widespread presence of heterogeneous nucleators (Murray et al., 2012; Pal et al., 2025). Classical Nucleation Theory describes the thermodynamics of embryo formation (Cui et al., 2023). The Gibbs free- energy change for forming an ice cluster of radius $r$ is given by

$$\Delta G=\Delta G_{bulk}+\Delta G_{surface}=-\frac{4}{3}\pi r^3\Delta G_v+4\pi r^2\gamma \quad (1)$$

https://doi.org/10.5194/egusphere-2026-3704
Preprint. Discussion started: 10 July 2026


where $\Delta G_v=\Delta\mu/\Omega$ is the volumetric free-energy change, $\Delta\mu=\mu_{vapor}-\mu_{ice}$ is the chemical-potential driving force per molecule, $\Omega=1/n_{ice}$ is the molecular volume in the ice Ih lattice, and $\gamma$ is the ice–vapor interfacial energy. For subcritical clusters ($r<r_c$), the surface-energy term dominates, rendering $\Delta G$ positive and the embryo thermodynamically unstable (Zhang et al., 2012). Once the critical radius

$$r_c=\frac{2\gamma}{\Delta G_v}=\frac{2\gamma\Omega}{\Delta\mu} \quad (2)$$

is exceeded, the volume term prevails and $\Delta G$ decreases, enabling spontaneous growth. The nucleation barrier is $\Delta G^*=\Delta G(r_c)$. In heterogeneous nucleation, the effective interfacial energy is reduced by the substrate, thereby lowering both $r_c$ and $\Delta G^*$ and facilitating ice formation at lower supersaturations.

Successful nucleation yields an initial hexagonal prism characteristic of ice Ih, the thermodynamically stable phase at atmospheric pressure (Llombart et al., 2020). Early growth produces micrometer-scale single crystals that quickly develop facets to minimize surface free energy, yet often retain structural imperfections, such as stacking faults or asymmetries inherited from nucleation. These defects can spread, leading to twinning and the development of arrowhead or crossed-plate shapes (Libbrecht, 2019a). In natural clouds, initial prisms usually reach 10–50 μm before diffusion-limited instabilities and anisotropic facet competition become dominant.

The steady-state nucleation rate $J$ can be approximated as

$$J=J_0\exp\left(-\frac{\Delta G^*}{k_BT}\right) \quad (3)$$

where $J_0$ is the pre-exponential factor, determined by the molecular collision frequency and the areal density of nucleation sites on the substrate; $\Delta G^*$ is the critical free-energy barrier, which is substantially reduced in heterogeneous nucleation (Akhtar et al., 2023).

In essence, atmospheric nucleation acts as the key interfacial gateway from vapor supersaturation to a faceted Ih prism. Although nucleation-induced imperfections may affect later morphology, the underlying hexagonal symmetry remains, providing the crystallographic framework that guides all subsequent diffusion- and kinetics-controlled development.

### 2.2 Diffusion and Attachment Kinetics

Vapor diffusion and surface attachment kinetics are the two main processes that limit the rate of vapor-phase snow crystal growth at the ice–vapor interface. Water vapor molecules move toward the crystal surface through diffusion, driven by ice supersaturation (Fig. 1d). Under typical atmospheric conditions, the steady-state vapor density around the crystal is described by the diffusion equation.

$$\nabla^2 n=0 \quad (4)$$

https://doi.org/10.5194/egusphere-2026-3704
Preprint. Discussion started: 10 July 2026


where $n$ is the number density of water molecules in air. Since latent-heat release is only a minor perturbation compared to mass diffusion, the isothermal approximation is valid. This allows the problem to be reformulated in terms of the dimensionless supersaturation field $\sigma$:

$$\nabla^2\sigma=0. \tag{5}$$

For steady-state growth the time derivative vanishes, reducing the equation to Laplace's equation. This approximation is justified because the characteristic diffusion relaxation time (about $R^2/D$) is orders of magnitude shorter than the timescale of appreciable crystal size change (about $R/v$), where $D$ is the water-vapor diffusion coefficient, $R$ the crystal radius, and $v$ the normal growth velocity.

The boundary condition at the ice-vapor interfaces is modified by the Gibbs-Thomson effect, which accounts for curvature-dependent vapor pressure:

$$\sigma_{\mathrm{surf}}=\frac{2\gamma\Omega}{k_B T R} \tag{6}$$

where $\gamma$ is the ice-vapor interfacial energy, $\Omega=1/n_{\mathrm{ice}}$ is the volume of a single water molecule, $n_{\mathrm{ice}}$ the molecular number density of ice, $k_B$ Boltzmann's constant, $T$ temperature, and $R$ the local radius of curvature of the convex surface. Far from the crystal, $\sigma \to \sigma_\infty$.

At the interface, impinging molecules must overcome an attachment barrier before integrating into the lattice (Fig. 1e). This kinetic process is measured by the attachment coefficient $\alpha$—the likelihood that a molecule adheres rather than desorbs. The molecular-scale dynamics include admolecule surface diffusion, terrace nucleation, step attachment, the Ehrlich–Schwoebel barrier, deposition, and sublimation (Fig. 1f). The net flux of water vapor to the surface is described by the modified Hertz–Knudsen equation (Libbrecht, 2012a)

$$F=\frac{\alpha v_{kin}}{4} c_{\mathrm{sat}}\sigma_{\mathrm{surf}}, \tag{7}$$

where $\alpha$ is the surface attachment coefficient, $v_{kin}=\sqrt{\frac{8k_BT}{\pi m}}$ is the mean thermal velocity, $m$ the mass of a water molecule, $c_{\mathrm{sat}}$ is the saturation number density of water vapor at the ice surface, and $\sigma_{\mathrm{surf}}$ is the local supersaturation at the ice-vapor interface. The corresponding normal growth velocity of the ice surface is

$$v_{\mathrm{n}}=\frac{F}{n_{\mathrm{ice}}} \tag{8}$$

In the pure diffusion-limited regime ($\alpha \to 1$), the analytical solution of Laplace's equation for a spherical crystal yields the far-field supersaturation profile

$$\sigma(r)=\sigma_\infty\left(1-\frac{R}{r}\right) \tag{9}$$

where $\sigma_\infty$ is the dimensionless far-field ice supersaturation, $R$ is the radius of the spherical ice crystal, and $r$ is the radial distance from the crystal center.

https://doi.org/10.5194/egusphere-2026-3704
Preprint. Discussion started: 10 July 2026


Substituting the radial gradient into the mass-flux continuity equation yields the normal radial growth velocity for a spherical crystal in the pure diffusion-limited regime (where attachment kinetics are negligible)

$$v_n = \frac{D c_{sat}}{n_{ice}} \frac{\sigma_\infty}{R}. \tag{10}$$

For the mixed kinetic-diffusion growth regime, where surface attachment kinetics exert a non-negligible limiting effect on growth, the normal growth velocity is given by:

$$v_n = \frac{\alpha v_{kin} c_{sat} \sigma_{surf}}{4 n_{ice}}. \tag{11}$$

When attachment kinetics are rate-limiting, the mixed kinetic–diffusion regime is characterized by matching the diffusive flux to the kinetic boundary condition, thereby reducing interfacial supersaturation.

$$\sigma_{surf} = \frac{\sigma_\infty}{1 + \frac{\alpha R v_{kin}}{4D}}. \tag{12}$$

This kinetic suppression of $\sigma_{surf}$ is the essential mechanism that stabilizes faceted growth against diffusion-driven morphological instabilities. When fully coupling water vapor diffusion, surface attachment kinetics, and latent heat transport effects (Libbrecht, 2016), the mixed-control growth velocity for a spherical crystal in the diffusion-limited regime is,

$$v_n = \frac{D c_{sat}}{n_{ice}} \frac{\sigma_\infty}{R} \frac{1}{1+\chi}, \tag{13}$$

where $\chi$ is the dimensionless parameter that quantifies latent-heat inhibition of growth. Under typical tropospheric conditions for natural snow crystals, $\chi \ll 1$. This confirms that latent-heat release exerts negligible inhibition, rigorously justifying the isothermal approximation used in snow-crystal growth models and cloud-microphysics parameterizations.

### 2.3 Facet Anisotropy of Snow Crystals

The pronounced morphological diversity of snow crystals mainly results from the strong temperature-dependent anisotropy in attachment kinetics between basal and prism facets (Fig. 1b) (Libbrecht, 2023). Examples of this variation are shown in Fig. 2.

https://doi.org/10.5194/egusphere-2026-3704
Preprint. Discussion started: 10 July 2026



**Figure 2: Representative polymorphic forms of snow crystals include: (a) columnar habits primarily influenced by prism-facet growth; (b) hexagonal plates formed under basal-facet dominance; (c) sector and star plates exhibiting early basal-surface instabilities; (d) stellar and fern-like dendrites created by diffusion-limited branching; (e) rare 12-branched forms resulting from synchronized perturbations at prism corners; (f) polycrystals assembled through multiple nucleation events.**

For a hexagonal ice Ih prism, the aspect ratio $A=c/a$, where $c$ is the dimension along the c-axis and $a$ along the a-axis, is directly determined by the relative normal growth velocities of the prism and basal facets:

$$A=\frac{c}{a} \propto \frac{v_{\text{basal}}}{v_{\text{prism}}} \propto \frac{\alpha_{\text{basal}}}{\alpha_{\text{prism}}}, \tag{14}$$

where $v_{\text{prism}}$ and $v_{\text{basal}}$ are the normal growth velocities of prism and basal facets, respectively, and $\alpha_{\text{prism}}$ and $\alpha_{\text{basal}}$ are the facet-specific attachment coefficients for each surface. This scaling relation quantitatively accounts for the well-known temperature-dependent habit transitions: near -15°C, $\alpha_{\text{prism}} \gg \alpha_{\text{basal}}$, producing thin plates with $A \ll 1$; near -5°C, $\alpha_{\text{basal}} \gg \alpha_{\text{prism}}$ favoring columnar habits with $A \gg 10$.

The time evolution of the aspect ratio under constant conditions follows from integration of the facet-specific growth rates:

$$A(T)=\frac{c_0+\int_0^t v_{\text{basal}}(t')\,dt'}{a_0+\int_0^t v_{\text{prism}}(t')\,dt'}, \tag{15}$$

where $a_0$ and $c_0$ are the initial crystal lengths along the a-axis and c-axis. The normal growth velocity follows the modified Hertz–Knudsen relation $v_n=\alpha v_{\text{kin}}\sigma_{\text{surf}}$. Precision chamber measurements confirm that $\alpha_{\text{prism}}$ peaks near -5°C, while $\alpha_{\text{basal}}$ reaches its minimum, precisely matching observed habit boundaries (Libbrecht, 2021b).

This facet-specific anisotropy has direct atmospheric effects: dual-view imaging reveals that the aspect ratio mainly controls terminal fall speed, with plate-like crystals ($A$~0.1) falling much more slowly than columnar crystals ($A$>5) of similar maximum size (Vázquez-Martín et al., 2021). These observations support better ice-hydrometeor parameterizations in

https://doi.org/10.5194/egusphere-2026-3704
Preprint. Discussion started: 10 July 2026


numerical weather and climate models, where habit-dependent fall speeds play a crucial role in determining cloud lifetime, precipitation efficiency, and radiative transfer.

### 2.4 The Tripartite Coupling Framework

Snow-crystal growth and morphological changes result from the nonlinear interaction of three interconnected elements: (1) the ice crystal itself, (2) water vapor as the growth material, and (3) background atmospheric substances such as air molecules, trace gases, aerosols, and particulates. These interactions, shown in Fig. 3, establish a comprehensive tripartite framework that connects microscopic interfacial processes with large-scale environmental boundary conditions.

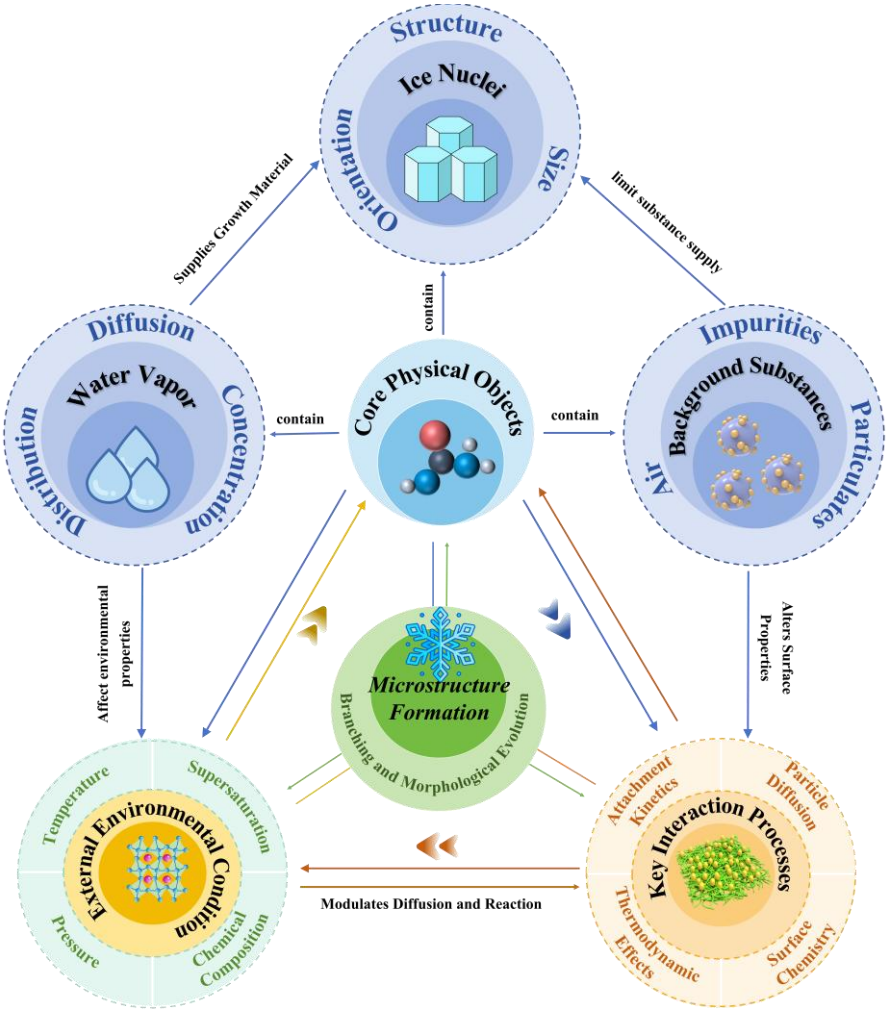


**Figure 3: Tripartite coupling framework for vapor-phase snow crystal growth and morphological polymorphism. The diagram emphasizes the three core entities (ice crystal, water vapor, and background atmospheric substances), external boundary conditions (temperature, supersaturation, pressure, chemical composition), and the key kinetic–thermodynamic feedback loops that control habit transitions, instability amplification, and the final crystal morphology.**

https://doi.org/10.5194/egusphere-2026-3704
Preprint. Discussion started: 10 July 2026


Within this framework, the ice crystal functions both as a product and a regulator: its crystallographic facets determine specific surface energies and attachment sites, while its size, curvature, and orientation influence the local diffusion field. Water vapor provides the $H_2O$ molecules needed for lattice incorporation, and background constituents act as both transport media and modulators of interfacial energetics through physisorption, chemisorption, and surface poisoning. Bidirectional couplings create nonlinear feedback loops: environmental parameters control diffusion and attachment rates, while the evolving crystal microstructure, in turn, affects local supersaturation, the stability of the quasi-liquid layer, and impurity incorporation. The main interactions are summarized in Table 1.

**Table 1: Summary of key interactions among the three core objects in snow crystal growth**

| No | Category | Specific Reaction / Interaction | Primary Mechanism | Key Findings / Unknown Areas | Ref |
|---|---|---|---|---|---|
| 1 | Ice Crystal – Water Vapor | Vapor deposition ($H_2O(g) \rightarrow H_2O(s)$) | Molecular attachment at kink/step sites | Well-described by modified Hertz-Knudsen equation; $\alpha(T)$ strongly temperature-dependent | (Kuroda and Lacmann, 1982; Libbrecht, 2017; Schlesinger et al., 2020; Shi et al., 2025) |
| 2 | | Sublimation/evaporation ($H_2O(s) \rightarrow H_2O(g)$) | Molecular desorption | Equilibrium vapor pressure $p_{sat}(T)$ known precisely; exponential $T$-dependence | (Murphy and Koop, 2005; Feistel and Wagner, 2007) |
| 3 | | Surface diffusion of adsorbed molecules | 2D diffusion on terraces | Influences step propagation; rates and pathways still not fully quantified | (Sosso et al., 2016; Harrington and Pokrifka, 2021) |
| 4 | Ice Crystal – Background Gas | Physisorption of air molecules | van der Waals forces | Modifies surface energy and QLL thickness; effect on $\alpha$ not fully quantified | (Libbrecht, 2017; Kling et al., 2018; Nagata et al., 2019; Sibley et al., 2021) |
| 5 | | Chemisorption of reactive gases (HCl, $HNO_3$, etc.) | Chemical bonding | Strongly alters $\alpha$ and habit; mechanism complex | (Bartels-Rausch et al., 2014; Yettapu et al., 2025) |
| 6 | | Gas entrapment during rapid growth | Kinetic trapping | Affects optical/mechanical properties; poorly understood | (Kärcher and Basko, 2004) |
| 7 | Ice Crystal – Solid Impurities | Heterogeneous nucleation | Lowering nucleation barrier | Well-established (e.g., mineral dust, bacteria); quantitative models incomplete | (Pruppacher and Klett, 2010) |
| 8 | | Surface poisoning / site blocking | Occupation of active growth sites | Reduces $\alpha$; screening thresholds and selectivity unknown | (Libbrecht, 2005; Murray et al., 2015) |
| 9 | | Lattice incorporation (substitutional / interstitial) | Doping / defect formation | Almost unexplored for physical property changes | (Lupi et al., 2017; Mochizuki and Molinero, 2018; Stoll et al., 2021) |

https://doi.org/10.5194/egusphere-2026-3704
Preprint. Discussion started: 10 July 2026


| No | Category | Specific Reaction / Interaction | Primary Mechanism | Key Findings / Unknown Areas | Ref |
|---|---|---|---|---|---|
| 10 | | Collisional energy / momentum transfer | Gas-kinetic collisions | Described by kinetic theory | (Abbatt, 2003) |
| 11 | Water Vapor – Background Gas | Diffusion regulation | Brownian motion in background gas | Well-defined *D(T,P)* relationship; ideal gas model valid | (Abbatt, 2003; Seinfeld and Pandis, 2016) |
| 12 | | Pre-nucleation cluster formation | Transient clustering | Potential role in nucleation; experimental detection difficult | (Abbatt, 2003) |
| 13 | Water Vapor – Chemical Impurities | Hydration of ions/organics | Hydration shell formation | Reduces water activity; complex effect on growth | (Abbatt, 2003; Bartels-Rausch et al., 2014) |
| 14 | | Gas-phase acid-base reactions (e.g., $NH_3$ + $H_2O$) | Proton transfer / pH modification | Indirect effect via chemical composition; direct impact on growth largely unknown | (Abbatt, 2003; Bartels-Rausch et al., 2014) |
| 15 | Background Substances Mutual | Non-ideal multicomponent gas behavior | Molecular interactions | Air treated as effective medium; composition-ratio effects understudied | (Bartels-Rausch et al., 2014) |
| 16 | | Gas–particulate interactions (e.g., $SO_2$ on dust) | Surface modification of aerosols | Affects IN activity; quantitative chain to crystal growth unclear | (Bartels-Rausch et al., 2014; Maurais et al., 2025; Rapp et al., 2025) |
| 17 | Ice Crystal Self-interaction | Surface reconstruction / annealing | Minimization of surface free energy | Time/temperature dependence not well constrained | (Hidas et al., 2017) |
| 18 | | Dislocation formation and migration | Stress-induced defect motion | Major potential influence on macroscopic morphology | (Hidas et al., 2017) |
| 19 | | Stacking fault accumulation | Layer mis-stacking | Explains trigonal/arrowhead forms; formation kinetics poorly known | (Kuhs et al., 2012; Murray et al., 2015) |

In summary, snow-crystal polymorphism arises from nonlinear, cross-scale interactions among crystal structure, diffusive transport, impurity-driven surface chemistry, and kinetic–thermodynamic processes within the tripartite framework. While macroscopic diffusion and attachment kinetics are well characterized, microscopic mechanisms involving impurities, QLL dynamics, and defects remain active research areas. This framework provides a systematic, mechanistic basis for understanding multi-parameter control of snow-crystal morphology in laboratory and atmospheric settings.

https://doi.org/10.5194/egusphere-2026-3704
Preprint. Discussion started: 10 July 2026


## 3. Key Parameters Governing Polymorphism of Snow Crystals

Snow crystal polymorphism is governed by a hierarchy of environmental and interfacial factors within the tripartite coupling framework. Temperature exerts primary control by regulating quasi-liquid layer (QLL) premelting, terrace step energetics, and facet-specific attachment kinetics at the ice–vapor interface. This temperature dependence generates strong anisotropy between basal and prism facets, dictating habit transitions. Supersaturation provides the thermodynamic driving force and induces the transition from kinetically limited faceted growth to diffusion-limited instabilities such as branching and dendritic growth.

High-precision laboratory and in-situ observations have established that trace atmospheric impurities—organic compounds, salts, and mineral dust—act as potent secondary modulators. They alter interfacial energetics, QLL stability, and attachment coefficients, shifting habit-transition temperatures by several degrees Celsius. Additional factors, including external electric fields, ambient pressure (which modulates vapor diffusivity), and non-equilibrium disturbances such as rapid supersaturation changes or sedimentation-driven reorientation, introduce further nonlinear feedback at the ice–vapor interface. These effects, superimposed on the primary variables, reveal the inadequacy of traditional two-parameter models and the necessity of the tripartite framework for mechanistic, multi-scale understanding of morphology.

### 3.1 Temperature

Temperature is the dominant control on snow crystal polymorphism. It regulates molecular-scale processes including QLL premelting, terrace step energetics, and facet-specific attachment kinetics at the ice–vapor interface. The attachment coefficient $\alpha(T)$ exhibits a non-monotonic, facet-dependent response, producing alternating regimes of basal versus prism dominance (Bailey and Hallett, 2004).

This sensitivity arises from abrupt changes in step free energy that govern two-dimensional nucleation rates and lateral step propagation. Near the melting point, a disordered QLL forms on the facets and lowers the kinetic barrier for attachment in a facet-specific manner (Libbrecht, 2017; Kling et al., 2018; Sibley et al., 2021). On basal facets, the QLL markedly reduces step free energy near −15 °C and enhances step mobility; on prism facets the effect is reversed, producing the classic habit reversals. At lower temperatures (below −20 °C), prism-facet attachment increases, restoring columnar dominance below −40 °C via kinetic roughening (Nagata et al., 2019; Llombart et al., 2020; Mochizuki et al., 2023; MacDowell, 2026).

https://doi.org/10.5194/egusphere-2026-3704
Preprint. Discussion started: 10 July 2026


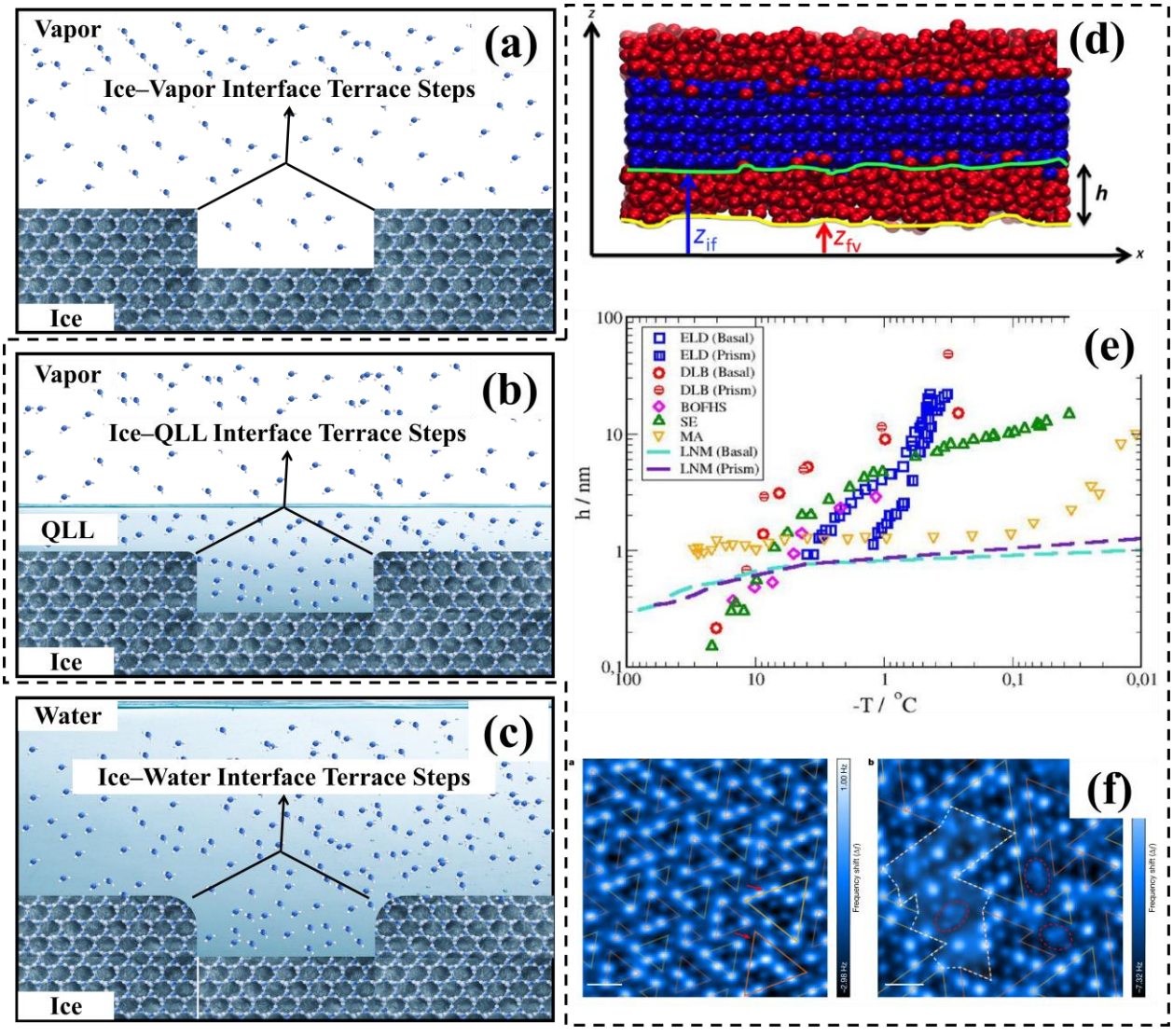


**Figure 4: QLL dynamics and facet-specific premelting at the ice–vapor interface. (a–c) Schematic terrace-step configurations: (a) Ice/vapor—sharp, ordered steps with high kinetic barriers at low temperatures; (b) Ice/QLL—a disordered premelt layer reduces barriers; (c) Ice/water—complete wetting smooths steps further. (d) Molecular-dynamics snapshot (TIP4P/ice) showing liquid-like (red) and solid-like (blue) regions (Llombart et al., 2020). (e) QLL thickness versus supercooling, compiled from experiments (ELB: Elbaum et al., 1993; DLB: Dosch et al., 1995; BOFHS: Bluhm et al., 2002; SE: Sadtchenko and Ewing, 2002; MA: Mitsui and Aoki, 2019) and TIP4P/ice simulations (LNM: Llombart et al., 2020). (f) Constant-height AFM images showing the onset of surface disorder at 123 K and coexistence of partially liquid-like structures at 125 K (Kling et al., 2018; Llombart et al., 2020; Yasuda et al., 2024; Hong et al., 2024; MacDowell, 2026). Source: Schematic panels created by the authors; experimental, simulation, and microscopy data/images adapted from Elbaum et al. (1993), Dosch et al. (1995), Bluhm et al. (2002), Sadtchenko and Ewing (2002), Kling et al. (2018), Mitsui and Aoki (2019), Llombart et al. (2020), Hong et al. (2024), Yasuda et al. (2024), and MacDowell (2026), with reuse permissions or applicable open licences verified where required.**

https://doi.org/10.5194/egusphere-2026-3704
Preprint. Discussion started: 10 July 2026


The QLL thickness follows the universal premelting scaling law:

$$h_{\mathrm{QLL}} \propto (T_{\mathrm{m}}\text{-}T)^{-1/3} \tag{16}$$

where $T_{\mathrm{m}}$ is the equilibrium melting point and $T_{\mathrm{m}}-T$ is the degree of supercooling. The scaling predicts rapid thickening near $T_{\mathrm{m}}$ and sharp thinning at lower temperatures, both of which modulate attachment barriers. Simulations (Fig. 4d) and experiments (Fig. 4e, f) reveal pronounced anisotropy between basal and prism facets, establishing the QLL as the principal mechanistic switch that selects which plane grows faster and thus determines habit.

Current $\alpha(T)$ parameterizations remain largely empirical and neglect impurity effects on QLL stability. First-principles predictions of facet-specific kinetics will require ab initio simulations under realistic tropospheric conditions.

### 3.2 Supersaturation

Supersaturation is the secondary control on morphological complexity. Once facet-specific attachment kinetics have established the initial hexagonal prism, supersaturation amplifies diffusion-limited instabilities. At low ice supersaturation ($\sigma < 0.05$), growth remains kinetically stabilized and yields compact faceted plates or columns. Moderate supersaturation ($0.05 < \sigma < 0.15$) triggers the Mullins–Sekerka instability: curvature-driven vapor fluxes at corners create positive feedback that destabilizes the interface and promotes dendritic branching, particularly near −15 °C. At high supersaturation ($\sigma > 0.25$), polycrystalline aggregates and secondary nucleation dominate, whereas moderate supersaturation below −30 °C favors single-crystal bullet rosettes.

The instability arises from nonlinear coupling among curvature-dependent diffusion, the Gibbs–Thomson effect, and facet-specific attachment kinetics. Lower $\alpha$ reduces kinetic stabilization of flat facets, allowing perturbations to grow at lower supersaturation thresholds and shifting the critical wavelength for branch initiation (Libbrecht, 2005; Lamb et al., 2023). Laboratory observations show that the supersaturation threshold for branching decreases with falling temperature as $\alpha$ declines. Fig. 5 illustrates the positive feedback: a small surface perturbation protrudes into the supersaturated vapor, attracting enhanced diffusive flux and accelerating local growth.

https://doi.org/10.5194/egusphere-2026-3704
Preprint. Discussion started: 10 July 2026


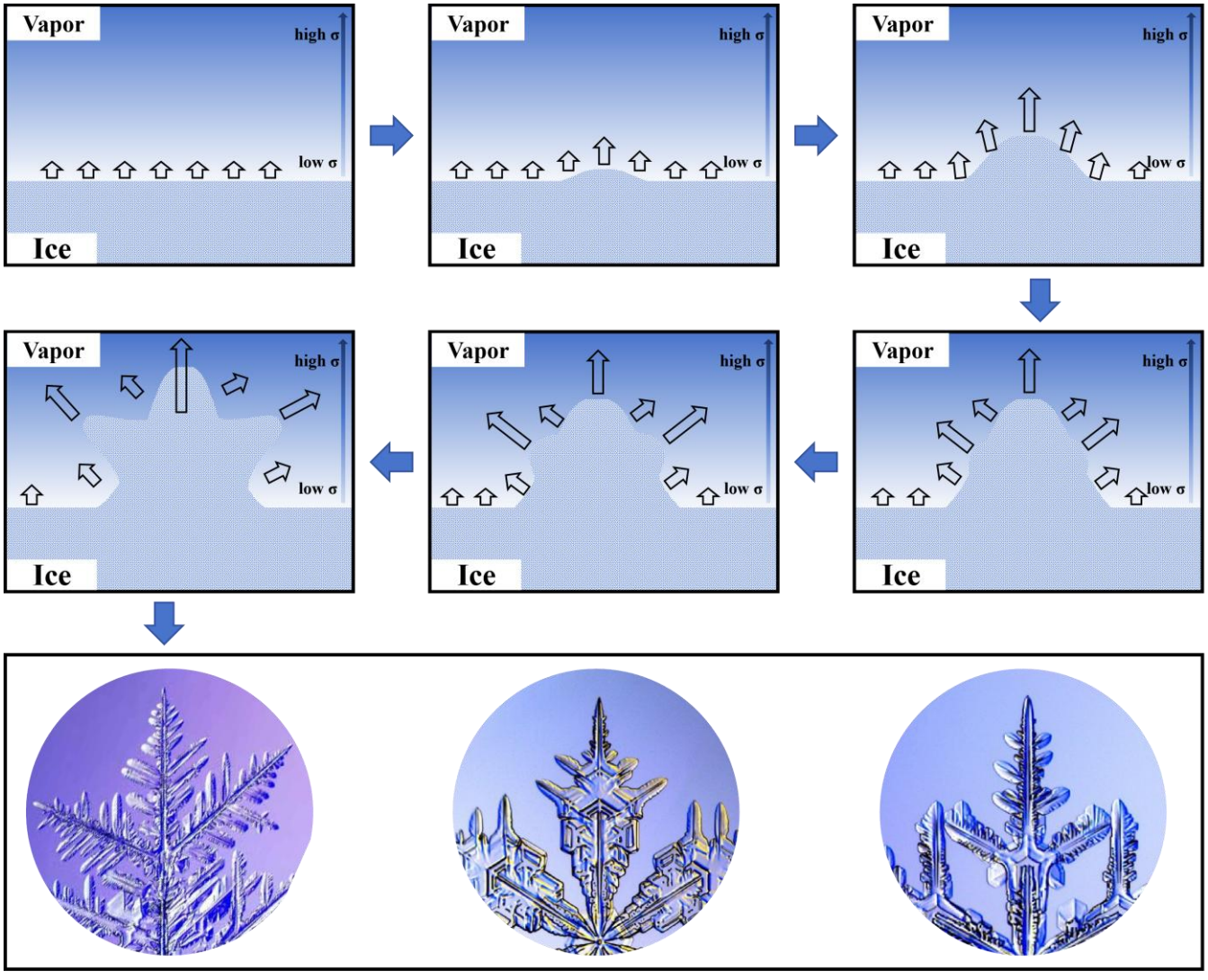


**Figure 5: Mullins–Sekerka instability during vapor-phase snow crystal growth. Upper panels illustrate the positive-feedback mechanism (Shimada et al., 2020): a small surface perturbation protrudes into supersaturated vapor, attracting enhanced diffusive flux and accelerating local growth. Lower panels show laboratory-grown crystals exhibiting the resulting dendritic branching.**

Molecular dynamics simulations show that at high supersaturation, QLL dynamics at branch tips locally modify facet-specific $\alpha$, thereby influencing tip radius and branching angles through interaction with the diffusion field (Sosso et al., 2016). Supersaturation thus supplies the thermodynamic drive while actively tuning the kinetic–diffusive balance that controls the faceted-to-branched transition.

In summary, supersaturation sets the thresholds for morphological instability, whereas temperature governs facet anisotropy. Their interplay within the tripartite framework accounts for the hierarchical complexity of natural snow crystals.

https://doi.org/10.5194/egusphere-2026-3704
Preprint. Discussion started: 10 July 2026


### 3.3 Structural Factors

Structural attributes of a snow crystal—size, crystallographic orientation, and accumulated defects—generate inherent nonlinear feedback within the tripartite framework. These attributes modulate local vapor supply, facet exposure, curvature, and defect propagation, thereby reinforcing or deviating from the habit set by temperature and supersaturation.

#### 3.3.1 Crystal Size

Larger crystals develop thicker concentration boundary layers during growth and sedimentation, lowering effective supersaturation at the ice–vapor interface. For a spherical approximation the vapor-density perturbation decays as $\exp(-r/\delta)$, where boundary-layer thickness $\delta \approx 2R/Sh$ and $Sh$ is the Sherwood number. Under typical atmospheric Reynolds numbers ($Re \approx 10$–$100$), $Sh$ lies between 2 and 10, so $\delta$ grows from ~50 μm for 100 μm crystals to several hundred micrometers for millimeter-sized crystals (Libbrecht, 2017; Vázquez-Martín et al., 2021). Consequently, normal growth velocity $v_n$ declines with size because of vapor depletion, favoring compact habits at later stages (Libbrecht, 2012b; Libbrecht, 2017; Libbrecht, 2019a; Libbrecht, 2019c).

The Gibbs-Thomson effect further inhibits growth of nanoscale-to-microscale crystals by raising equilibrium vapor pressure over convex surfaces:

$$\Delta\sigma_{\mathrm{curv}} = \frac{2\gamma\Omega}{Rk_BT}, \tag{17}$$

where $\gamma \approx 0.109$ J/m² is the ice–vapor surface energy, $\Omega = 3.26\times10^{-29}$ m$^3$ is the molecular volume of ice (from $\rho_{\mathrm{ice}} \approx 917$ kg/m$^3$), $k_B$ is Boltzmann's constant, and $T$ is temperature. For crystals tens of micrometers across, the curvature effect is negligible; thin boundary layers maintain high effective supersaturation and promote diffusion-limited Mullins–Sekerka instability and dendritic branching (Demange et al., 2017).

Beyond diffusion-driven morphological instabilities, a second core mechanism governs the fine-scale faceted evolution of snow crystals: the edge-sharpening instability (ESI) driven by structure-dependent attachment kinetics (SDAK) (Libbrecht, 2013; Libbrecht, 2019a).

As the uppermost terrace narrows, its effective attachment coefficient $\alpha$ increases. When terrace width $w$ becomes much smaller than the characteristic SDAK length $\lambda$ (typically 0.1–1 μm), $\alpha$ approaches unity because nearly all adatoms reach the step edge before desorbing. The resulting acceleration of edge growth further narrows the terrace, establishing a positive feedback loop that drives rapid narrowing and disappearance (Libbrecht, 2012b; Libbrecht, 2017). ESI quantitatively accounts for the abrupt formation of thin plates near −15 °C and hollow columns near −5 °C (Fig. 6) (Libbrecht, 2013; Libbrecht, 2019a).

https://doi.org/10.5194/egusphere-2026-3704
Preprint. Discussion started: 10 July 2026


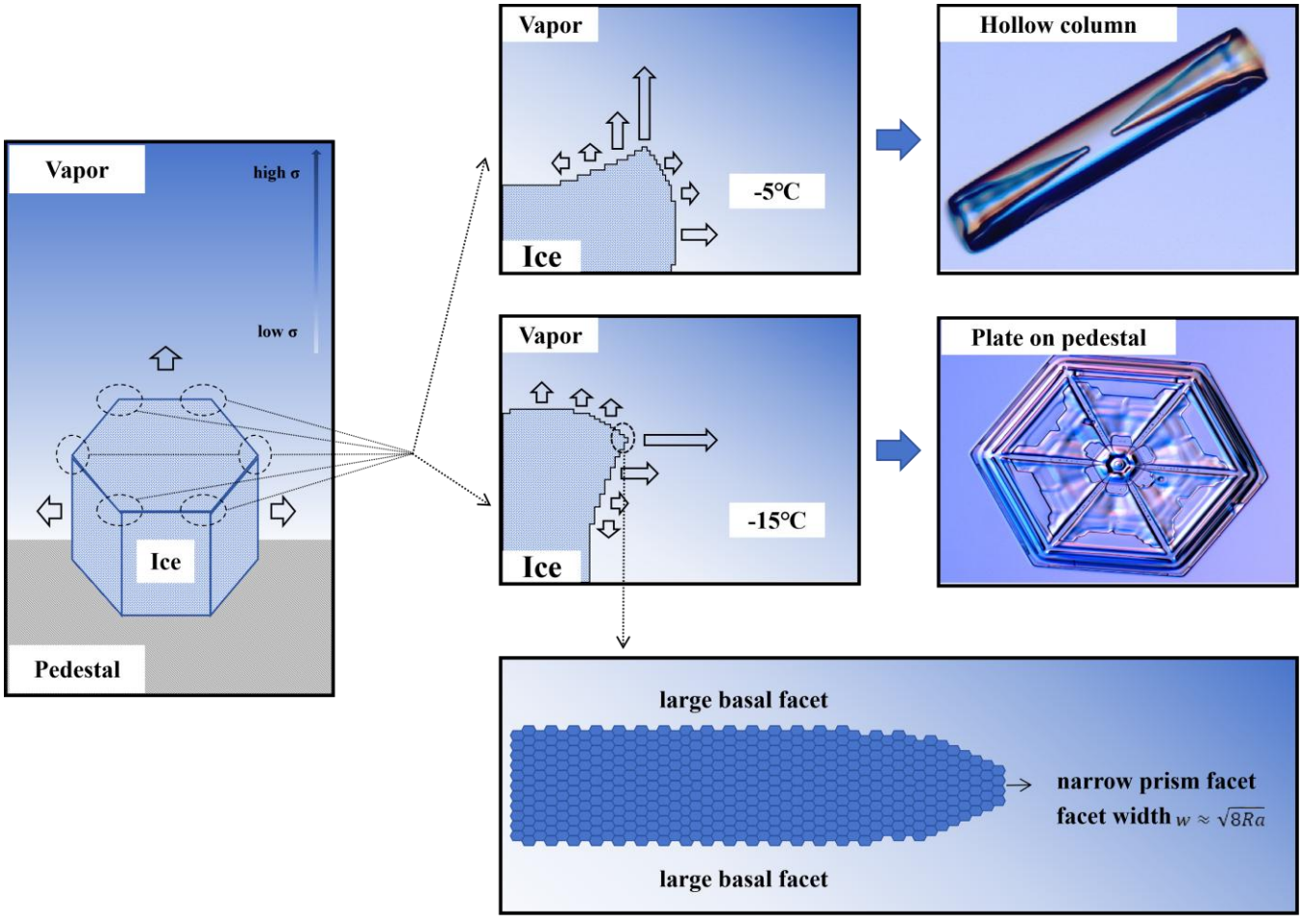


**Figure 6: Edge-sharpening instability (ESI) driven by structure-dependent attachment kinetics (SDAK) (Libbrecht, 2012b; Libbrecht, 2019a; Libbrecht, 2019c). Upper panel: formation of hollow columns at −5 °C. The trapezoidal prism facets narrow progressively; the SDAK mechanism increases α at the edges, creating a positive feedback loop that sharpens the edges and promotes columnar growth. Lower panel: formation of plates on pedestals at −15 °C. Basal facets likewise undergo edge sharpening and plate-like growth through SDAK-driven positive feedback. The relation $w \approx \sqrt{8Ra}$ (where w is prism-facet width at the plate edge, R is edge curvature radius, and a is the water-molecule size) quantitatively describes the geometry.**

Laboratory growth-rate measurements and phase-field simulations confirm that small crystals (<100 μm) exhibit unstable branched growth at high effective supersaturation, whereas larger crystals (>500 μm) stabilize into compact shapes once diffusion limitations dominate (Demange et al., 2017; Libbrecht, 2019a, b, c).

### 3.3.2 Crystal Orientation

During sedimentation, snow crystals orient their largest projected area perpendicular to the flow to maximize aerodynamic drag. Thin plates and stellar dendrites fall horizontally, exposing prism facets to the highest vapor flux and thereby

https://doi.org/10.5194/egusphere-2026-3704
Preprint. Discussion started: 10 July 2026


promoting plate-like growth. Columnar crystals fall vertically, aligning the c-axis with the flow and facilitating elongation. This orientation-dependent exposure generates a secondary feedback that modulates Reynolds and Sherwood numbers, boundary-layer thickness, and effective attachment kinetics (Vázquez-Martín et al., 2021).

### 3.3.3 Defect Accumulation

Growth history imprints lasting structural defects—stacking faults, dislocations, and surface irregularities—that shape subsequent development. Basal-plane stacking faults induce twinning and break symmetry, yielding trigonal or arrowhead forms even within the hexagonal Ih lattice (Libbrecht, 2021b; Mohammadian et al., 2021). Dislocations migrate to the ice–vapor interface and serve as persistent step sources that control branch spacing and symmetry (Table 1). These defects interact with QLL dynamics and attachment kinetics, amplifying deviations from idealized habits. Fig. 7 shows representative malformed crystals, including crossed plates from twinning, arrowhead twins from stacking faults, irregular plates from lattice defects, split stars from ESI, crossed needles from polycrystalline seeds, and polycrystalline aggregates from mid-fall sintering.

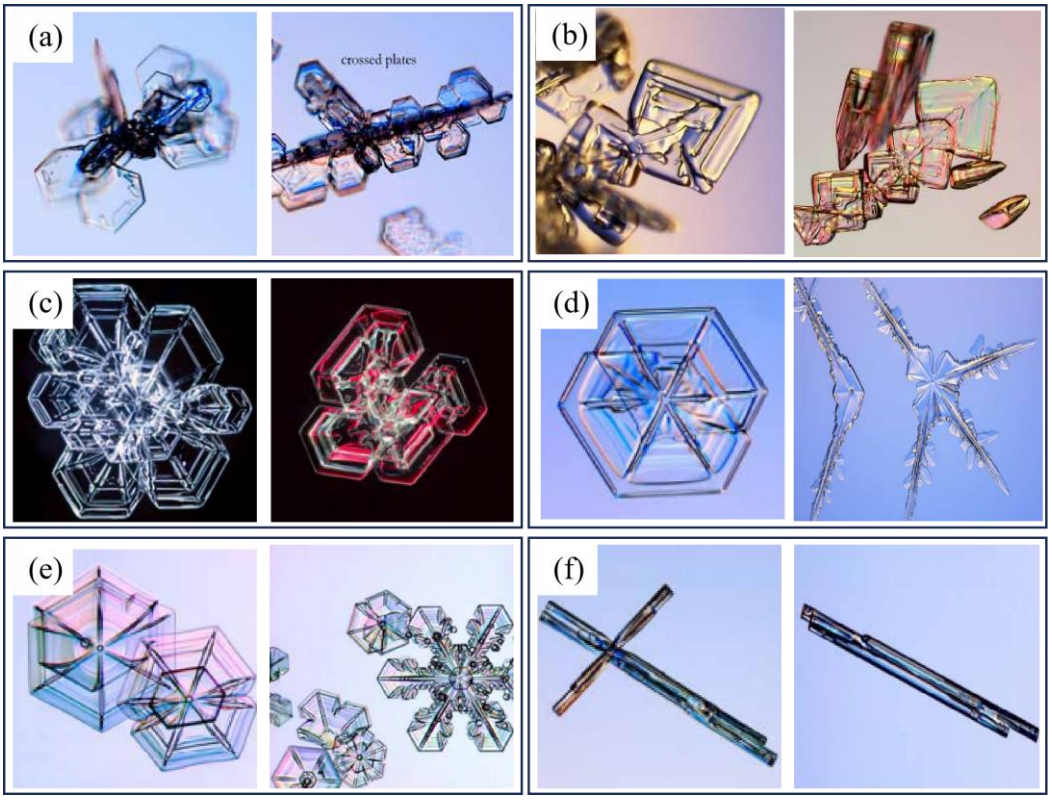


**Figure 7: Gallery of malformed snow crystals shaped by growth history and defect accumulation (Bailey and Hallett, 2004). (a) Crossed plates from twinning; (b) arrowhead twins from basal-plane stacking faults; (c) irregular plates from lattice defects and impurity adsorption; (d) split stars from ESI; (e) crossed needles from polycrystalline seeds or collisions; (f) polycrystalline aggregates from mid-fall sintering.**

https://doi.org/10.5194/egusphere-2026-3704
Preprint. Discussion started: 10 July 2026


In summary, structural factors generate nonlinear feedback within the tripartite framework: crystal size modulates vapor supply and curvature, orientation controls facet-specific flux, and defects impart a crystallographic memory that biases branching and symmetry. These self-regulating mechanisms explain many deviations from classical habit diagrams in laboratory and atmospheric settings.

### 3.4 Modulating Factors

Beyond temperature and supersaturation, secondary environmental and chemical influences shape snow crystal polymorphism by modulating facet-specific attachment kinetics, step free energy, QLL stability, and the local vapor diffusion field within the tripartite framework. These factors introduce nonlinear effects that shift habit-transition temperatures, generate rare morphologies, and increase deviations from idealized diagrams.

#### 3.4.1 Chemical Impurities and Aerosols

Trace impurities—sulfates, organic compounds, biological aerosols, and mineral dust—preferentially adsorb on basal or prism facets, locally altering interfacial energetics and $\alpha$. Even low concentrations can shift habit-transition temperatures by several degrees Celsius through surface poisoning, step pinning, and QLL modulation. Organic vapors, for example, selectively inhibit basal-facet attachment and promote needle-like growth, whereas mineral dust enhances heterogeneous nucleation and alters step-propagation barriers.

#### 3.4.2 Air Pressure and Vapor Diffusivity

Ambient pressure influences the water-vapor diffusion coefficient ($D \propto 1/P$ under isothermal conditions). At lower pressures (e.g., 500 hPa in the upper troposphere) D roughly doubles, extending the diffusion length and shifting growth from diffusion-limited to kinetically limited regimes. This suppresses Mullins–Sekerka branching and favors compact, faceted morphologies. Higher pressures enhance diffusion limitation and promote open dendritic structures. The effect is particularly relevant for cirrus-cloud crystals and planetary ice under low-pressure conditions.

#### 3.4.3 Electric Fields

Externally applied electric fields provide a controllable means to modulate interfacial attachment kinetics. In the electric-needle technique, a high positive voltage applied to a frost-covered wire lowers equilibrium vapor pressure at the charged tip via electrostatic self-energy, producing a spatial gradient in $\alpha$. This drives a runaway sharpening instability, forming slender needles with sub-micron radii (Bartlett et al., 1963; Libbrecht and Tanusheva, 1998; Libbrecht et al., 2002; Libbrecht, 2021b). Molecular polarization effects largely cancel at first order, so surface-charge-induced vapor-pressure reduction is the dominant mechanism. Removal of the voltage leaves a well-defined seed that continues to grow into complex plates or dendrites according to ambient temperature and supersaturation (Fig. 8).

https://doi.org/10.5194/egusphere-2026-3704
Preprint. Discussion started: 10 July 2026


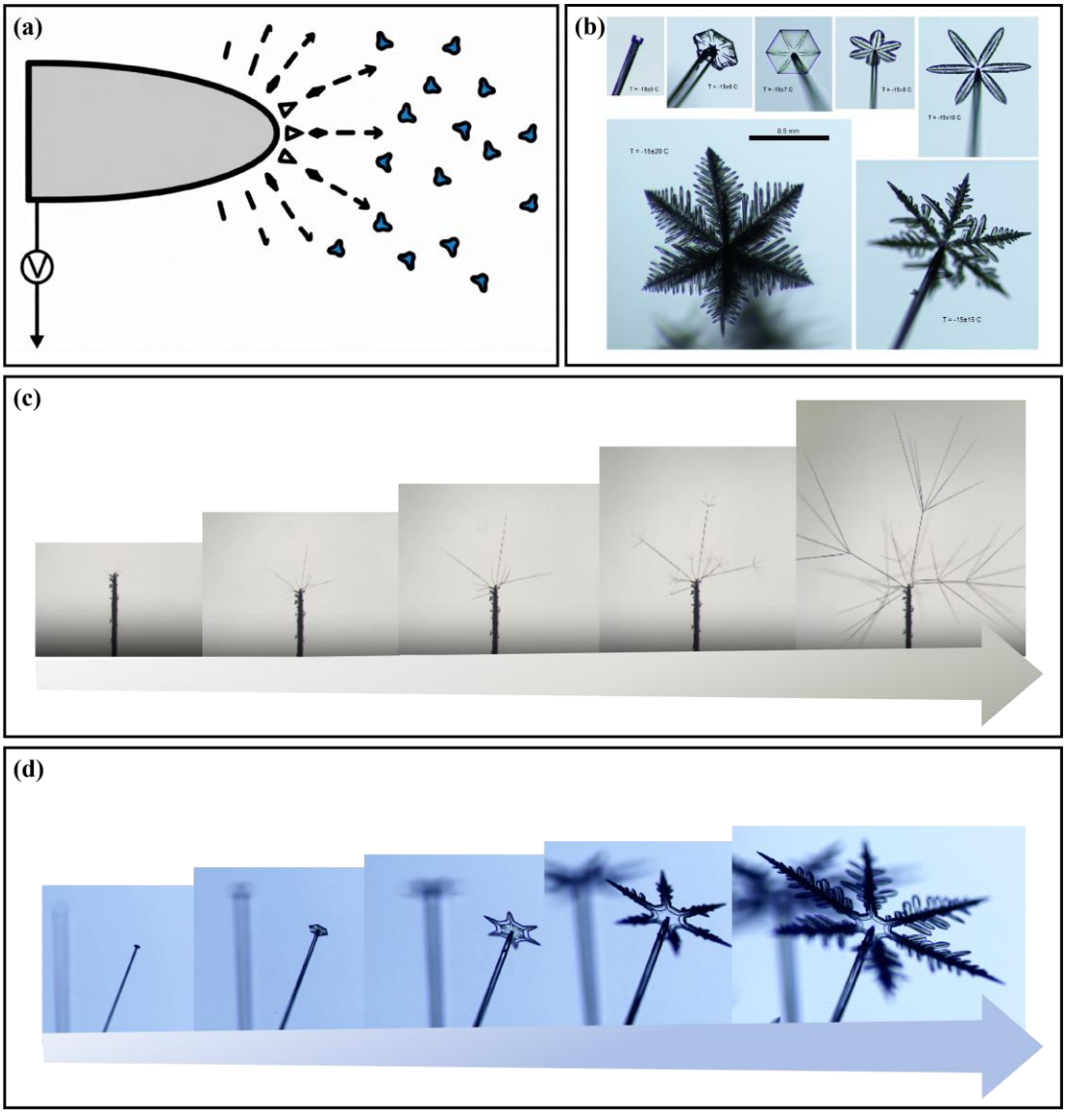


**Figure 8: Electrically induced growth instability and electric ice-needle formation (Libbrecht and Tanusheva, 1998; Libbrecht et al., 2002; Libbrecht, 2021b; Libbrecht, 2022). (a) Principle: electrostatic self-energy reduces equilibrium vapor pressure at the charged tip. (b) Resulting morphologies on electric needles. (c) Schematic of the dual-diffusion-chamber setup. (d) Time-lapse sequence showing transition from needle to dendritic or plate-like forms after voltage removal.**

In summary, modulating factors fine-tune growth by altering $\alpha$, step energetics, QLL stability, and diffusion fields. Impurities modify surface chemistry, pressure regulates mass transport, and electric fields impose spatial kinetic anisotropy. Superimposed on the primary temperature–supersaturation controls, these secondary influences produce the full spectrum of observed morphologies and underscore the value of the tripartite framework for predictive modeling under realistic conditions.

https://doi.org/10.5194/egusphere-2026-3704
Preprint. Discussion started: 10 July 2026


## 4. Microscopic Mechanisms of Polymorphic Snow Crystals

The morphological diversity of vapor-grown snow crystals originates in microscopic interfacial physics at the ice–vapor interface. Integration of high-precision laboratory measurements, molecular dynamics simulations, and in-situ atmospheric observations has yielded quantitative, mechanistically grounded explanations for the full range of natural and laboratory morphologies (Ball, 2011; Schlesinger et al., 2020). This section focuses on the mechanisms of facet competition, diffusion-limited and kinetically driven instabilities, symmetry breaking, and characteristic interfacial growth features within the tripartite coupling framework of ice crystal, water vapor, and background atmospheric substances (including trace impurities). Recent advances have converted earlier phenomenological descriptions into a unified, predictive physical model that links molecular-scale processes directly to macroscopic crystal shapes (Libbrecht, 2013, 2017).

### 4.1 Primary Morphological Classifications

Snow crystal classification has advanced over four centuries from qualitative descriptions to mechanism-based taxonomies grounded in ice-growth physics (Barnard, 2024). Ancient Chinese records noted six-petaled symmetry (Han Ying, ~135 BC; Zhang Heng, second century AD) (Needham and Lu, 1959; Xu, 2009). Western study began with Kepler's 1611 analysis of hexagonal symmetry (Ball, 2011) and Descartes' 1637 observations (Ping, 2016). Bentley's 19th-century photomicrographs documented their diversity (Bentley and Humphreys, 1931). Modern systems began with Nakaya's 1930 habit diagram and expanded through Magono and Lee's 1966 taxonomy (80 types) (Nakaya, 1954; Magono and Lee, 1966), later simplified to ~35 core types (Libbrecht, 2022), and most recently to 121 types by Kikuchi et al. (2013) incorporating polar observations. These early efforts laid the foundation for quantitative classification.

Nakaya's 1930 diffusion-chamber experiments yielded the first habit diagram (41 types). Magono and Lee (1966) established the widely used 80-type meteorological taxonomy. Later mechanistic understanding reduced the system to ~35 core types (Libbrecht, 2022). Global observations, especially in polar regions, led Kikuchi et al. (2013) to a comprehensive 121-type framework that includes low-temperature forms.

These developments are summarized in Fig. 9, which traces the evolution from early qualitative observations to modern mechanistic classification systems.

https://doi.org/10.5194/egusphere-2026-3704
Preprint. Discussion started: 10 July 2026


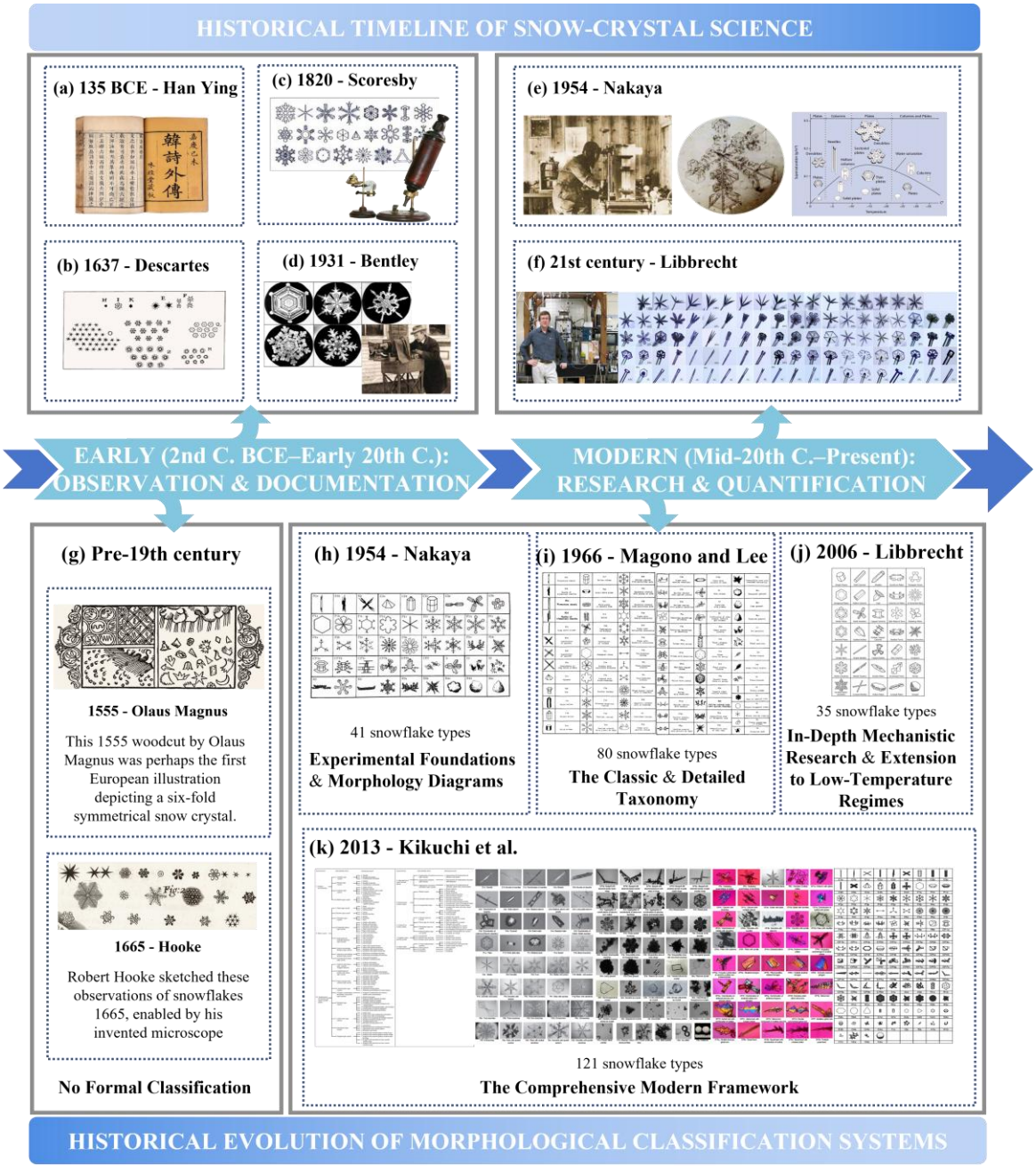


**Figure 9: Historical timeline of snow-crystal science and evolution of morphological classification systems, illustrating the progression from early qualitative observations and documentation (2nd century BCE–early 20th century) to modern research and quantification (mid-20th century–present), along with the refinement of snow crystal taxonomies over four centuries. Source: Timeline and layout created by the authors; historical and classification materials reproduced/adapted from Needham and Lu (1959), Xu (2009), Bentley and Humphreys (1931), Nakaya (1954), Magono and Lee (1966), Kikuchi et al. (2013), Barnard (2024), and Libbrecht (2022), with reuse permissions or applicable licences verified where required.**

https://doi.org/10.5194/egusphere-2026-3704
Preprint. Discussion started: 10 July 2026


Despite the fine-grained subtypes in modern taxonomies, nearly all vapor-grown snow crystals observed in nature and in the laboratory fall into four primary morphological categories. These categories organize the discussion and are illustrated in Fig. 10: (1) simple faceted morphologies (prisms, plates, and columns); (2) complex plate-like dendrites (sector plates and stellar dendrites); (3) complex columnar morphologies (hollow columns, needles, and bullet rosettes); and (4) special and rare morphologies (trigonal crystals, trident forms, and negative crystals).

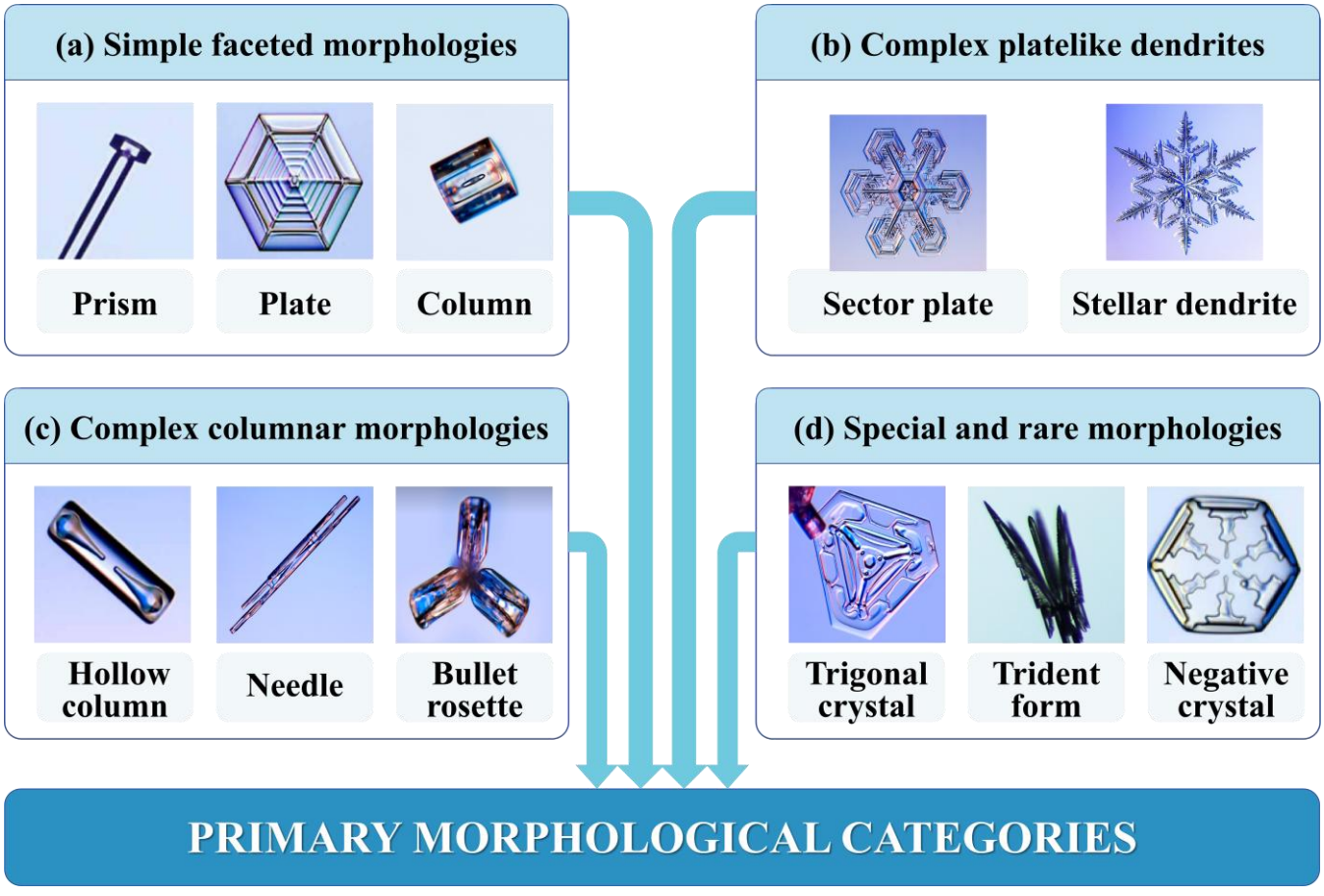


**Figure 10: Primary morphological categories of vapor-grown snow crystals, serving as the organizational framework for this section.**

The complete morphological development from an initial ice nucleus to fully branched structures is shown schematically in Fig. 11, highlighting key transitional stages: hexagonal plates, sectored plates, ridge and rib formation, inward-growing growth rings, and the onset of dendritic sidebranching. Each phase is driven by specific interfacial mechanisms—facet-specific attachment kinetics, diffusion-limited instabilities, edge-sharpening instability (ESI), and structural feedback—within the tripartite coupling framework.

https://doi.org/10.5194/egusphere-2026-3704
Preprint. Discussion started: 10 July 2026


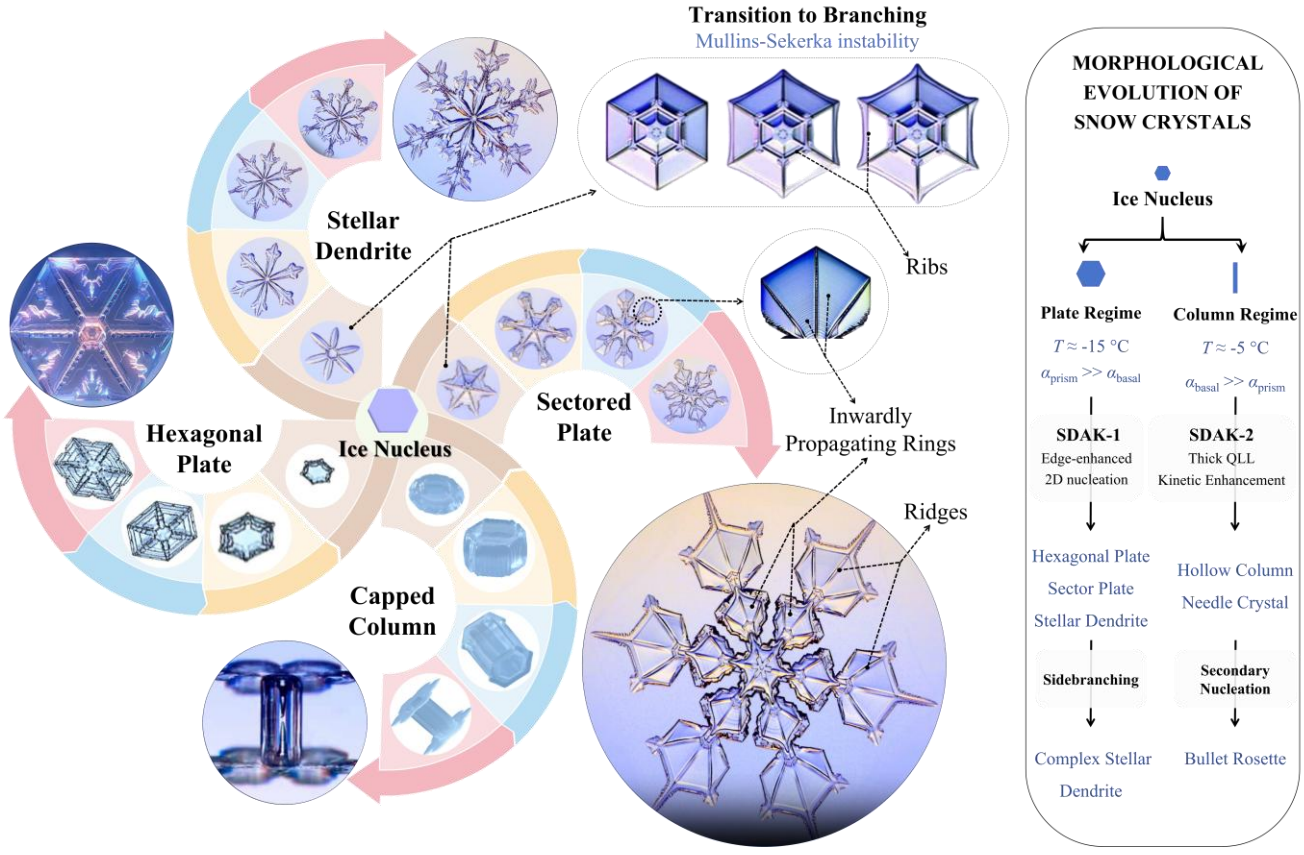


**Figure 11: Morphological evolution of snow crystals from the initial ice nucleus to complex branched forms. Schematic illustration of progressive stages, including hexagonal plates, sectored plates, stellar dendrites, capped columns, ridge and rib development, inwardly propagating growth rings, and the onset of dendritic sidebranching.**

### 4.1.1 Simple Morphologies: Prisms, Plates, and Columns

The basic structure of all vapor-grown snow crystals is the hexagonal ice Ih prism that forms immediately after nucleation (Llombart et al., 2020). It is bounded by two basal {0001} facets (perpendicular to the c-axis) and six symmetry-equivalent prism $\{10\bar{1}0\}$ facets (parallel to the c-axis). This geometry reflects the tetrahedral hydrogen-bond network of the ice Ih lattice, which produces distinct surface energies and facet-specific attachment kinetics. Under low to moderate supersaturation, habit is determined solely by temperature-dependent competition between the two facet types via the attachment coefficient $\alpha$.

Near −15 °C and −2 °C (classic plate-like regimes), prism-facet dominance ($\alpha_{prism} \gg \alpha_{basal}$) drives rapid lateral expansion along the a-axis, producing thin hexagonal plates with extreme aspect ratios ($A = c/a \ll 1$). These plates reach diameters of 0.5–5 mm and thicknesses of only 10–100 μm because basal-facet attachment is strongly suppressed. Near −5 °C and below −40 °C (classic columnar regimes), basal-facet dominance produces slender prismatic columns with $A \gg 10$. Hollow-column

https://doi.org/10.5194/egusphere-2026-3704
Preprint. Discussion started: 10 July 2026


variants arise when ESI accelerates attachment at facet edges relative to central basal regions, trapping vapor pockets and forming internal cavities 10–200 μm in diameter. Typical growth rates for these simple faceted forms are 0.1–1 μm/s, with facet-specific velocities differing by factors of 10–100 depending on temperature, consistent with precision diffusion-chamber data (Libbrecht, 2017).

#### 4.1.2 Complex Platelike Dendrites: Sector Plates, Stellar Dendrites

As supersaturation increases beyond the low regime, diffusion-limited Mullins–Sekerka instabilities amplify small corner perturbations, producing complex plate-like dendrites. Sector plates emerge first, with distinct hexagonal sectors separated by elevated ridges. Higher supersaturation yields stellar dendrites with highly branched arms. In well-developed stellar dendrites, each primary arm has a prominent central ridge (an elevated longitudinal spine) flanked by parallel ribs (secondary striations perpendicular to the arm axis). These ribs arise from periodic Mullins–Sekerka instabilities along the advancing edge, with typical spacing of 5–20 μm (most often 10–15 μm). Rib spacing matches the wavelength of the fastest-growing instability mode and increases with supersaturation. Both ridges and ribs enhance structural rigidity and influence light-scattering properties. Diameters typically range from 0.5 to 5 mm, with exceptional specimens reaching 10 mm, depending strongly on ambient supersaturation and growth duration.

#### 4.1.3 Complex Columnar Morphologies: Hollow Columns, Needles, and Bullet Rosettes

In columnar growth regimes, increasing supersaturation drives a transition from solid columns to more complex forms. Hollow columns develop when ESI accelerates attachment at basal-facet edges relative to flatter central regions, trapping vapor pockets inside. Needles (extremely slender columns) form under strong basal-facet dominance at very low temperatures or in strong electric fields, yielding high length-to-width aspect ratios. Bullet rosettes arise from secondary nucleation of branchlets on a central prismatic seed, typically at supersaturations >25% and temperatures below −40 °C. Although they appear polycrystalline, bullet rosettes are single-crystal structures; their branches often develop hollow interiors by the same ESI mechanism. Overall growth rates in these regimes are slower (0.01–0.1 μm/s), but localized edge velocities are substantially higher, consistent with molecular-dynamics simulations of step-propagation barriers.

#### 4.1.4 Special and Rare Morphologies: Trigonal Snow Crystals, Trident Forms, and Negative Snow Crystals

Trigonal and trident crystals exhibit stable three-fold symmetry despite the underlying six-fold hexagonal lattice of ice Ih. Their formation arises from stacking-fault-induced kinetic asymmetry in the basal plane: an initial stacking fault creates a persistent growth bias in which one set of three prism facets grows faster than the others. This asymmetry is amplified and stabilized by diffusion competition and vapor shielding, yielding robust trigonal morphologies (Libbrecht and Arnold, 2009b; Libbrecht, 2021a). The formation mechanism of triangular and trident-shaped snow crystals is illustrated schematically in Fig. 12. Induced side-branching—achieved by temporarily lowering supersaturation to facet the tip and then raising it—

https://doi.org/10.5194/egusphere-2026-3704
Preprint. Discussion started: 10 July 2026


synchronizes branch initiation at the three active prism corners and produces highly symmetric patterns (Libbrecht, 2017, 2019a).

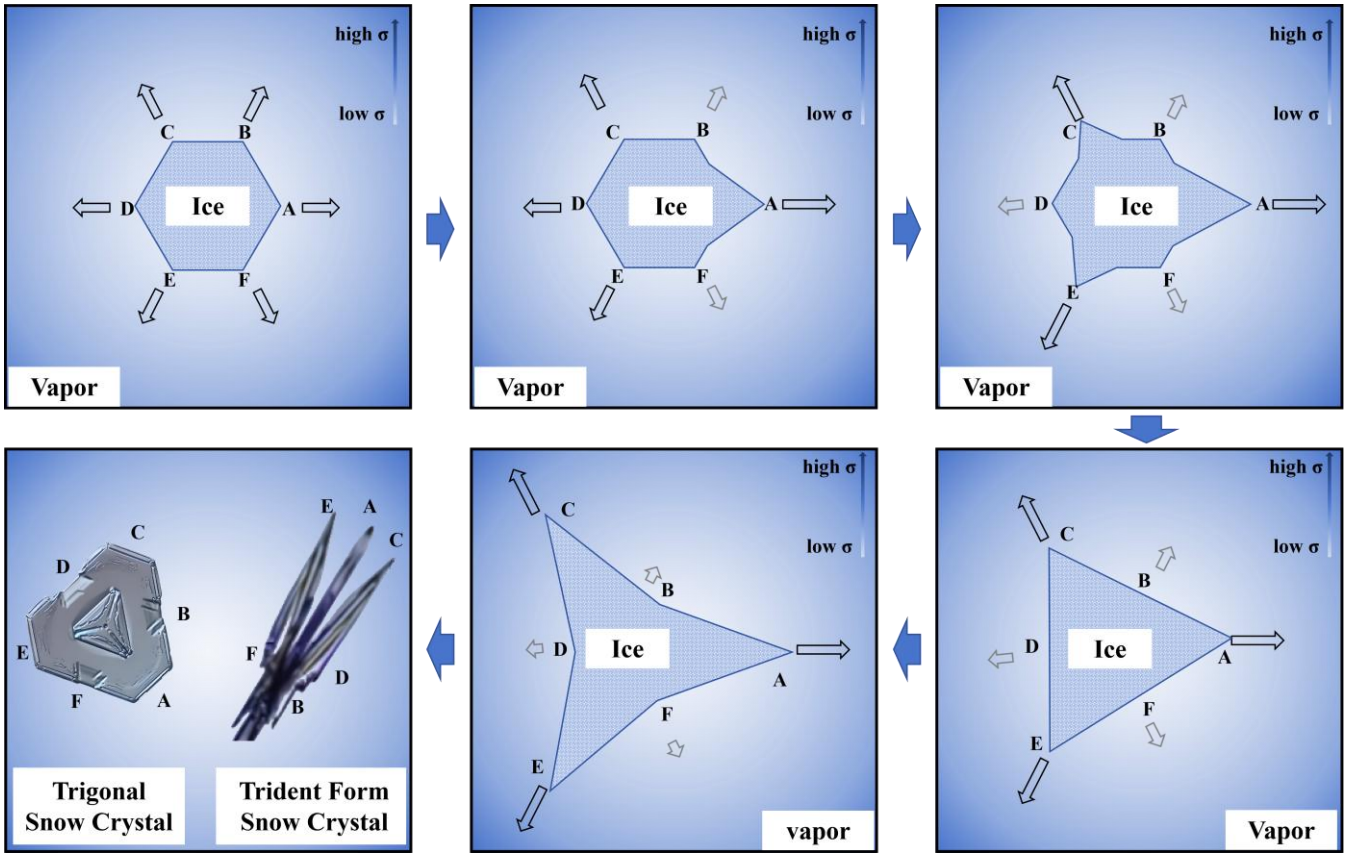


**Figure 12: Schematic of the formation mechanism of triangular and trident-shaped snow crystals. Among the six primary branches extending from a columnar crystal, branch A is slightly longer than the others. Due to the tip effect, water-vapor supersaturation around it is high (high σ), leading to preferential growth of A. Adjacent branches B and F lie in the shadow region of A (low σ), inhibiting their growth. As A continues to grow, B and F become further shaded, while branches C and E (initially positioned farther back) become exposed to higher supersaturation (high σ) and grow more rapidly, simultaneously suppressing D. Eventually, branches A, C, and E dominate, forming a trident shape, while B, D, and F are strongly shaded and nearly cease to grow. This process results in triangular and trident-shaped snow crystals.**

In 2021, Libbrecht achieved nearly 100% trigonal crystal formation at −14 °C and 107% ice supersaturation by applying controlled surface perturbations to slender ice needles (Libbrecht, 2021a). This landmark experiment resolved a long-standing puzzle in ice physics: kinetic asymmetry—whether from stacking faults or deliberate surface modification—can suppress three of the six prism facets, producing stable trigonal growth that persists throughout development.

Negative snow crystals (internal voids) form through localized sublimation–deposition cycles that parallel normal growth. These faceted cavities, bounded by slow-growing planes, typically occur in columnar or plate-like crystals under fluctuating

https://doi.org/10.5194/egusphere-2026-3704
Preprint. Discussion started: 10 July 2026


supersaturation, with diameters of 10–200 μm (Libbrecht, 2017). High sublimation barriers on flat facets kinetically freeze their shapes, preserving well-defined crystallographic faces.

The four main categories and their transitional stages demonstrate that snow crystal shapes arise from the combined effects of facet-specific attachment kinetics, diffusion-limited instabilities, edge-sharpening instability, and structural feedback within the tripartite coupling framework. The following sections examine these microscopic mechanisms in detail and provide a unified physical explanation for the full range of observed habits.

### 4.2 Unified Explanation of Morphological Diversity

All observed snow crystal morphologies emerge from a single unified physical framework: the Comprehensive Attachment Kinetics (CAK) model, whose core is the Structure-Dependent Attachment Kinetics (SDAK) description (Libbrecht, 2017, 2019a; Libbrecht and Walkling, 2023). Within this framework, crystal growth proceeds exclusively by two-dimensional layer nucleation and terrace-step propagation on faceted surfaces, with the facet-specific attachment coefficient set jointly by temperature, supersaturation, and the local mesoscopic geometry of the facet.

The Ehrlich–Schwoebel (E–S) barrier plays a central role in this layer-by-layer picture. It is the additional energy cost an admolecule must overcome to descend a step edge, arising from reduced coordination at the step riser. On a rigid ice lattice a large E–S barrier suppresses downward crossing, limiting admolecule transport across terraces and controlling 2D nucleation rates. Surface premelting and QLL formation soften the step structure, markedly reducing the E–S barrier and enabling long-range surface diffusion—an effect strongly amplified at sharp, narrow facets.

The SDAK model formalizes how local facet geometry modulates $\alpha$. For a facet of finite width $w$, the effective attachment coefficient is enhanced relative to its value on an infinite terrace ($\alpha_\infty$) according to

$$\alpha(w,T,\sigma)=\alpha_\infty(T,\sigma)+\Delta\alpha(T)\cdot\exp\left(-\frac{w}{\lambda(T)}\right) \tag{18}$$

where $\Delta\alpha(T)\approx 0.5$–$0.9$ is the maximum enhancement at vanishing width and $\lambda(T)\approx 0.1$–$1$ μm is the characteristic SDAK length scale. This exponential dependence on generates the positive feedback loop that drives the edge-sharpening instability (ESI): narrowing of the facet increases $\alpha$, which accelerates edge growth and further narrows the facet.

Two distinct, temperature-dependent microscopic pathways underlie the SDAK effect (Libbrecht, 2022) (Fig. 13).

**SDAK-1 (edge-enhanced 2D nucleation)** dominates in the plate-like regime near −15 °C, where the QLL is thin. At sharp edges, surface diffusion elevates local admolecule density on narrow facets, lowering the effective supersaturation barrier for 2D nucleation. The critical free-energy barrier is modified from its classical form to:

$$\Delta G^*(w)=\frac{\pi\gamma_{\text{step}}^2\Omega}{k_B T\ln(1+\sigma_{\text{eff}}(w))} \tag{19}$$

where $\sigma_{\text{eff}}(w)$ is the effective local supersaturation (which increases with decreasing w due to edge-enhanced admolecule accumulation), $\gamma_{\text{step}}$ is the step free energy; $\Omega$ is the molecular volume of ice; $k_B$ is the Boltzmann constant. A lower $\Delta G^*(w)$

https://doi.org/10.5194/egusphere-2026-3704
Preprint. Discussion started: 10 July 2026


increases the 2D nucleation rate exponentially, directly enhancing the effective attachment coefficient $\alpha$ on narrow facets. This mechanism is the primary driver of ESI and thin platelike growth near -15°C, the classic dendritic snow growth regime.

**SDAK-2 (QLL-mediated kinetic enhancement)** prevails in the columnar regime near −5 °C, where the QLL is thicker and more dynamic. At sharp facet edges, enhanced surface transport and localized latent-heat release thicken the QLL locally, increasing molecular mobility and reducing the kinetic barrier for incorporation into the ice lattice. This effect is quantified by the temperature-dependent kinetic prefactor $A(T, w)$ in the Arrhenius expression for the attachment coefficient:

$$\alpha(T,w)=A(T,w)\cdot \exp\left(-\frac{E_a(T,w)}{k_B T}\right) \tag{20}$$

where $E_a$ is the activation energy for molecular attachment, which decreases with increasing QLL thickness. Local thickening at narrow edges increases $A(T,w)$ and reduces $E_a$, enhancing $\alpha$. This mechanism drives hollow columns and needles near −5 °C.

At the heart of both pathways lies the E–S barrier (Fig. 13e), which functions as a temperature-dependent molecular switch. On rigid lattices the barrier is high and suppresses terrace transport; QLL formation softens the step edge, lowers the barrier, and enables efficient admolecule delivery to narrow facets, thereby activating SDAK. This bidirectional coupling between mesoscopic geometry and microscopic kinetics is the fundamental principle of the SDAK model. It provides a self-consistent, quantitative explanation for edge-sharpening instability, habit transitions between plate-like and columnar forms, and the full spectrum of snow crystal polymorphism.

By linking molecular-scale interfacial processes (step energetics, E–S barrier, QLL dynamics) directly to mesoscopic morphological evolution, the SDAK framework resolves long-standing discrepancies between classical diffusion-limited theory and experimental observations and offers a predictive foundation for snow crystal growth under realistic tropospheric conditions.

https://doi.org/10.5194/egusphere-2026-3704
Preprint. Discussion started: 10 July 2026


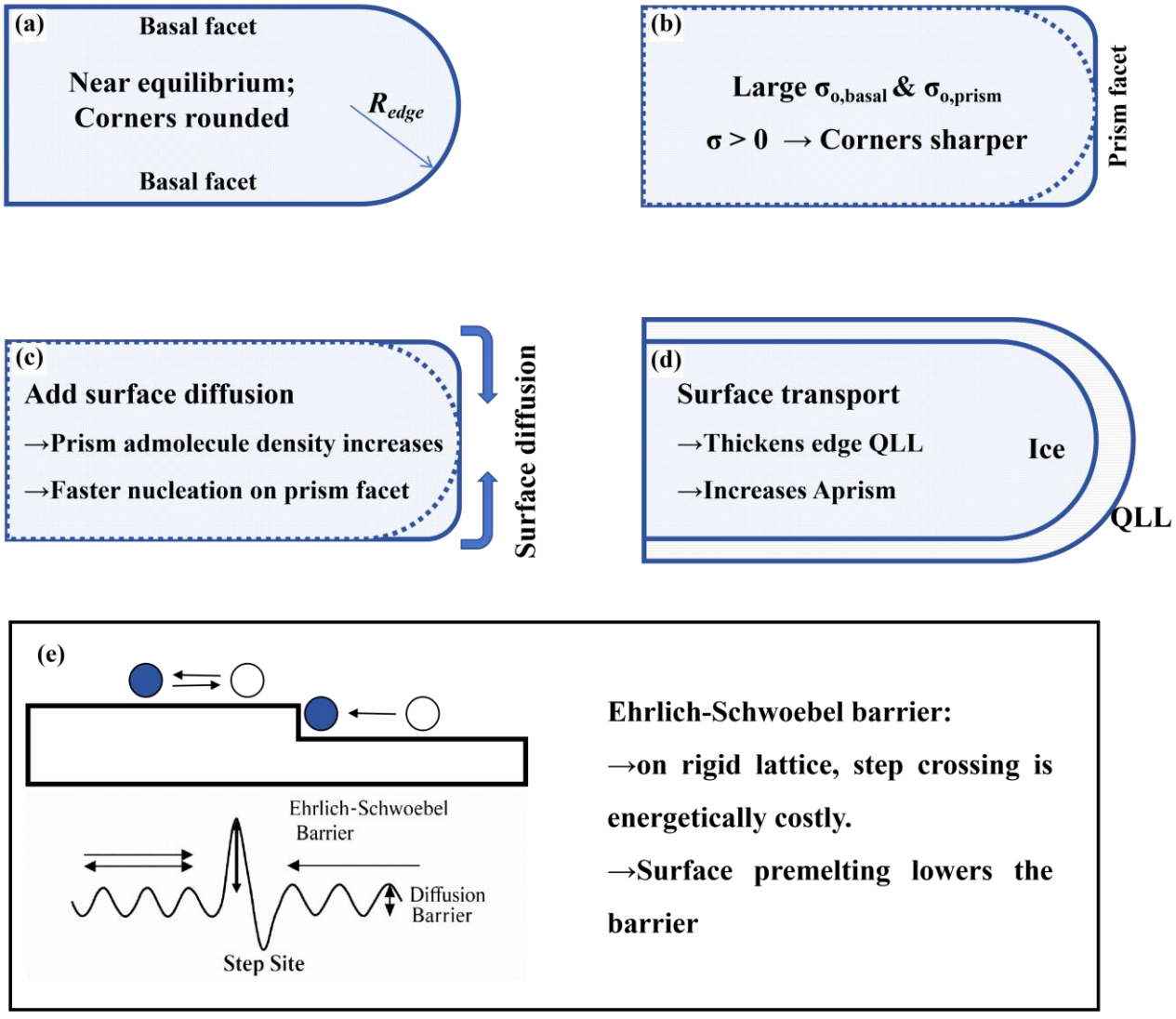


**Figure 13: Complete physical picture of Structure-Dependent Attachment Kinetics (SDAK) in snow crystal growth (Libbrecht, 2019b). (a) Basal facet near equilibrium. (b) Supersaturation-driven corner sharpening and facet narrowing. (c) SDAK-1: edge-enhanced admolecule density and 2D nucleation. (d) SDAK-2: QLL thickening and kinetic enhancement at sharp edges. (e) E–S barrier as the central molecular switch, strongly modulated by surface premelting.**

This unified mechanistic view demonstrates that snow crystal polymorphism is not the result of isolated environmental parameters but emerges from the nonlinear, cross-scale interplay of facet-specific attachment kinetics, diffusion fields, and structural feedback within the tripartite coupling framework.

https://doi.org/10.5194/egusphere-2026-3704
Preprint. Discussion started: 10 July 2026


### 4.3 Microscale Surface Features

In addition to macroscopic habit transitions governed by SDAK and diffusion-limited instabilities, characteristic microscale surface features—ribs, ridges, and inward-propagating rings—emerge during vapor-phase snow crystal growth. These features are direct experimental signatures of coupled step dynamics, curvature-dependent diffusion fields, impurity–step interactions, and Ehrlich–Schwoebel (E–S) barrier modulation at the ice–vapor interface (Fig. 14). They arise from nonlinear feedback between surface diffusion of admolecules, terrace-step propagation, and local supersaturation gradients, providing stringent tests of the SDAK model within the tripartite coupling framework.

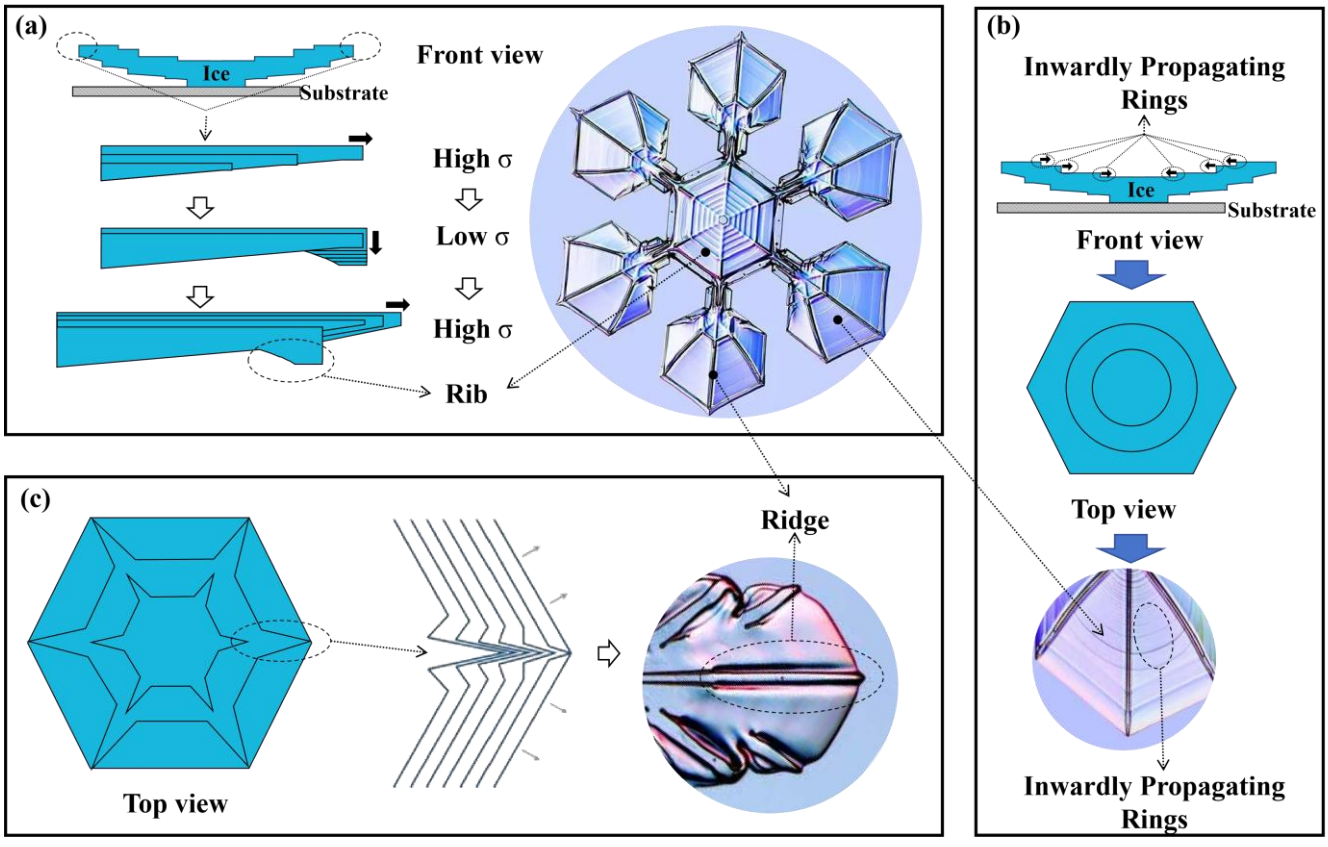


**Figure 14: Characteristic microscale surface features on vapor-grown snow crystals. (a) Rib formation on lower or edge surfaces via cyclic supersaturation fluctuations: high-σ phases drive rapid lateral extension, while low-σ phases induce localized thickening and produce transverse stepped ribs. (b) Inward-propagating rings on concave basal facets: converging step flow from radial diffusion gradients leads to step bunching and macroscopic concentric macrosteps (typical spacing 10–50 µm). (c) Gully-flanked radial ridges: corner-enhanced diffusion creates raised central ridges flanked by depleted gullies; impurity segregation at slower-growth zones can etch permanent linear depressions.**

Ribs develop primarily on the lower surfaces or facet edges of substrate-supported or sedimenting crystals through temporal fluctuations in local supersaturation. High-σ intervals promote rapid lateral extension, while subsequent low-σ intervals drive

https://doi.org/10.5194/egusphere-2026-3704
Preprint. Discussion started: 10 July 2026


localized vertical thickening via enhanced 2D nucleation on the lower terrace. Repeated cycles generate the characteristic transverse stepped rib morphology (Fig. 14a). This process is governed by the interplay between diffusion-field relaxation timescales and facet-specific attachment kinetics, with each rib recording a discrete perturbation in growth velocity. The E–S barrier plays a decisive role: its modulation by local QLL thickness controls the efficiency of adsorbed-molecule descent, stabilizing the bunched step configuration and locking in rib spacing.

Inward-propagating rings appear exclusively on concave crystal surfaces, where radial diffusion gradients drive converging step flow toward the facet center. Discrete atomic steps coalesce into macroscopic macrosteps through bunching instabilities (Fig. 14b). The bunching arises from competition between surface diffusion of adsorbed molecules and the E–S barrier, which impedes step descent and promotes step–step repulsion. As steps converge, the local curvature-induced supersaturation gradient further accelerates the leading step, producing visible concentric hexagonal rings with typical spacings of 10–50 μm. This phenomenon directly reflects the nonlinear coupling between diffusion-limited transport and interfacial kinetics and provides a mesoscopic manifestation of the SDAK-1 pathway on concave geometries.

Gully-flanked radial ridges develop on the upper concave faces of hexagonal plates and dendrites. Corner-enhanced vapor diffusion creates six prominent radial ridges (spines) that grow inward from the hexagonal corners (Fig. 14c). Convergence of lateral step flow toward the ridge axis raises the central spine, while step depletion on either side forms paired flanking gullies. In addition to this intrinsic diffusion-driven mechanism, trace impurities swept by advancing steps can segregate into slower-growth zones adjacent to the ridge, permanently etching linear depressions through surface-energy modification and step pinning. On convex surfaces the same Mullins–Sekerka instability produces analogous ridge-and-gully and rib structures, extending the framework from simple faceted plates to complex branched dendrites.

These microscale features collectively demonstrate that snow crystal morphology is sculpted not only by global temperature and supersaturation but also by mesoscopic feedback among step propagation, curvature-dependent diffusion fields, E–S barrier dynamics, and impurity-mediated surface chemistry. Quantitative analysis of rib spacing, ring periodicity, and ridge–gully geometry provides direct experimental validation of the SDAK model and the tripartite coupling framework, bridging molecular-scale interfacial processes to observable macroscopic architecture. Future high-resolution in-situ imaging combined with atomistic simulations will be essential to resolve remaining open questions on impurity–step selectivity and dynamic E–S barrier modulation under realistic tropospheric conditions.

### 4.4 Collective Growth Phenomena

As isolated faceted crystals evolve into interacting branch networks, collective growth phenomena emerge that cannot be captured by single-facet kinetics alone. At high supersaturation, side-branch merging and ice-bridge formation are closely related processes that illustrate how diffusion-field instabilities are amplified by facet-specific attachment kinetics to produce emergent structural complexity. The sequence is depicted in Fig. 15: initial diffusion-field overlap between approaching branches, ice-bridge formation via localized supersaturation gradients and secondary deposition, and progressive side-branch merging driven by positive feedback.

https://doi.org/10.5194/egusphere-2026-3704
Preprint. Discussion started: 10 July 2026


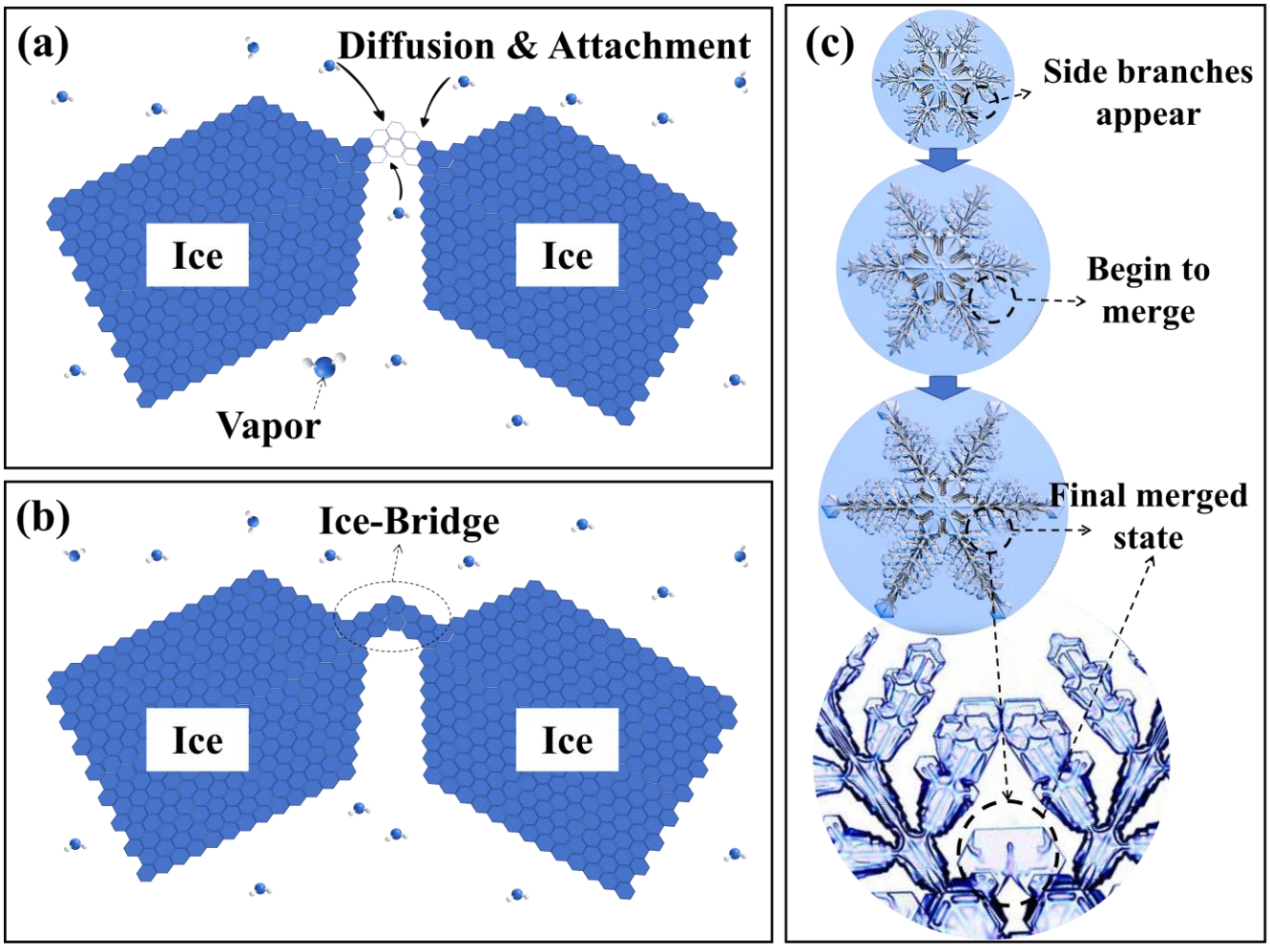


595

**Figure 15: Collective growth phenomena in snow crystal networks. (a) Initial diffusion-field overlap between approaching branches. (b) Ice-bridge formation via localized supersaturation gradients and secondary deposition. (c) Side-branch merging sequence, showing progressive gap closure and arm thickening driven by positive feedback.**

Side-branch merging occurs when adjacent branches coalesce through diffusion-field overlap in the inter-branch gap. As
600 branch spacing decreases, the steady-state supersaturation field ($\nabla^2\sigma = 0$, isothermal approximation) develops a steep gradient $|\nabla\sigma| \sim \sigma_\infty/d$ on the facing surfaces. This curvature-enhanced flux creates a positive feedback: accelerated local growth further narrows the gap, driving rapid coalescence and the formation of thicker primary arms or irregular dendritic networks (Kikuchi et al., 2013; Libbrecht, 2017; Shimada et al., 2020).

Ice-bridge formation lies on the same continuum but arises when complete merging is geometrically or temporally hindered
605 (e.g., in three-dimensional spatial dendrites or at moderately lower supersaturation). Transient supersaturation fluctuations or residual vapor in the confined inter-branch region enable localized two-dimensional nucleation or direct deposition across the gap, stabilizing thin crystalline connections (Curiotto et al., 2023). These bridges are reinforced by repeated sublimation–

https://doi.org/10.5194/egusphere-2026-3704
Preprint. Discussion started: 10 July 2026


deposition cycles and impurity-mediated step pinning, linking background atmospheric substances to mesoscopic architecture.

Kinetic Monte Carlo simulations of interdroplet ice-bridge formation during condensation frosting provide complementary atomic-scale insight (Curiotto et al., 2023). Bridge elongation kinetics exhibit a quadratic dependence on inter-particle distance and are dominated by surface diffusion and attachment rather than droplet size. This universality underscores that both merging and bridging arise from the same nonlinear coupling of diffusion-limited transport, facet-specific attachment kinetics, and E–S barrier modulation within the tripartite framework.

In summary, the full morphological diversity of snow crystals emerges from a hierarchical, multi-scale cascade within the tripartite coupling framework. At the molecular scale, facet-specific attachment kinetics—modulated by temperature-dependent step free energies, quasi-liquid layer dynamics, and the Ehrlich–Schwoebel barrier—establish the fundamental growth anisotropy. At the mesoscopic scale, vapor diffusion fields and instabilities (Mullins–Sekerka and edge-sharpening) amplify these anisotropies into faceted and branched patterns. At the macroscopic scale, collective phenomena such as side-branch merging and ice-bridge formation arise from dynamic interactions among neighboring structures, generating emergent complexity beyond isolated single-crystal growth. This unified perspective positions vapor-phase snow crystal growth as a paradigmatic example of non-equilibrium interfacial pattern formation in systems with strong kinetic anisotropy, resolving long-standing phenomenological puzzles and providing a predictive mechanistic foundation for laboratory experiments and atmospheric cloud microphysics modeling.

## 5. Applications and Interdisciplinary Extensions

Mechanistic insights from vapor-phase snow crystal growth—particularly the tripartite coupling framework, the Structure-Dependent Attachment Kinetics (SDAK) model, facet-specific attachment coefficients, and quasi-liquid layer (QLL) dynamics—extend well beyond basic interfacial science. These principles offer quantitative predictive power for a range of interdisciplinary applications, from atmospheric microphysics to engineered surfaces and planetary cryoscience (Vázquez-Martín et al., 2021; Dai et al., 2026). By connecting molecular-scale interfacial processes to macroscopic morphological outcomes, the framework supports targeted advances in climate modeling, passive icephobic technologies, and the interpretation of extraterrestrial ice structures.

### 5.1 Parameterization of Snow Crystals in Atmospheric and Climate Models

Accurate representation of ice crystal properties is essential for global climate and numerical weather prediction models. Snow crystal habit, size distribution, cross-sectional area, and fall speed directly influence cloud radiative properties, precipitation efficiency, and the vertical transport of water and latent heat (Pruppacher and Klett, 2010; Morrison et al., 2020; Seinfeld and Pandis, 2016; McMurdie et al., 2022; D'Acunzi et al., 2021; Gerber et al., 2022). Current parameterizations rely

https://doi.org/10.5194/egusphere-2026-3704
Preprint. Discussion started: 10 July 2026


on simplified habit diagrams and empirical fall-speed relationships, introducing notable uncertainties—particularly below −20 °C, where columnar and needle habits dominate.

High-resolution, shape-dependent fall-speed measurements (e.g., from dual-view imaging) show that the aspect ratio $A=c/a$—dictated by the ratio of facet-specific attachment coefficients $\alpha_{prism}/\alpha_{basal}$—is the dominant control on terminal velocity (Morrison et al., 2020; Vázquez-Martín et al., 2021). Incorporating SDAK-derived $\alpha(T)$ parameterizations and QLL-modulated kinetic anisotropy into microphysical schemes can substantially reduce biases in cirrus and mixed-phase cloud radiative forcing. These refinements also improve the treatment of ventilation effects and sedimentation-induced orientation changes, enabling more accurate simulations of cloud lifetime and precipitation under realistic dynamic conditions.

### 5.2 Engineering Applications of Snow Accumulation and Icephobic Surfaces

Snow crystal morphology and interfacial attachment kinetics are central to engineering challenges involving snow and ice accumulation on infrastructure, including photovoltaic panels, power transmission lines, wind turbine blades, and transportation systems. The transition between dry and wet snow—governed by heat exchange and liquid water content—critically influences adhesion strength and shedding behavior (Mohammadian et al., 2021; Huang et al., 2022; Chu et al., 2024)

Insights from facet-specific attachment kinetics and QLL dynamics directly inform the rational design of icephobic surfaces. Superhydrophobic and icephobic coatings exploit minimized solid–liquid contact area and delayed heterogeneous nucleation by mimicking the kinetic suppression mechanisms that stabilize faceted growth. Low-surface-energy nanostructures reduce effective contact area and disrupt QLL continuity, lowering ice adhesion while promoting passive shedding (Huang et al., 2022). Recent field-validated composite nanoporous superhydrophobic films on aluminum substrates have achieved a 95.7% reduction in rime ice mass over 120 hours of natural exposure, retaining 90.5% performance after one year of weathering (Dai et al., 2026). These advances pave the way for hybrid passive–active ice-protection systems that minimize energy consumption in aeronautical and energy applications.

### 5.3 Planetary Science and General Principles of Crystal Growth

Snow crystal polymorphism serves as a universal model for vapor-phase crystal growth under extreme conditions, with direct relevance to planetary science. On icy ocean worlds such as Europa and Enceladus, and on Mars, sublimation–condensation cycles under low pressure and temperature (<100 K) produce complex cryostructures whose morphologies encode information about subsurface oceans, cryovolcanic plumes, and trace volatiles (Porco et al., 2006; Roth et al., 2014; Postberg et al., 2018). Laboratory reproduction of these forms under analogous conditions, guided by SDAK and tripartite coupling principles, enables quantitative interpretation of remote-sensing and in-situ data on extraterrestrial frost and plume deposits.

More broadly, the interplay of diffusion-limited transport, facet-specific attachment kinetics, and morphological instabilities observed in snow crystals illustrates core principles of non-equilibrium solidification. The pronounced temperature

https://doi.org/10.5194/egusphere-2026-3704
Preprint. Discussion started: 10 July 2026


sensitivity of kinetic anisotropy makes ice a paradigmatic system for understanding pattern formation in materials science (thin-film growth and alloy solidification) and biomineralization. Future integration of ab initio-derived $\alpha(T)$ parameterizations with multi-scale modeling will extend these insights to predict crystal morphologies across vastly different planetary environments, advancing both fundamental interfacial physics and astrobiological exploration.

In summary, the mechanistic framework developed for snow crystal growth—anchored in the tripartite coupling among ice crystals, water vapor, and background substances—translates fundamental interfacial science into practical predictive tools for atmospheric modeling, passive anti-icing technologies, and planetary cryoscience. These applications underscore the power of interfacial kinetics to bridge molecular-scale processes with macroscopic outcomes in complex, non-equilibrium systems.

## 6. Conclusions and Outlook

Snow crystal polymorphism illustrates how subtle, temperature-sensitive molecular processes at the ice–vapor interface control large-scale pattern formation. Since Libbrecht's 2005 review identified attachment kinetics as the driver of habit transitions, two decades of advances have transformed the field from phenomenological descriptions to a quantitative, mechanistic framework grounded in interfacial physics.

Key advances include: (i) confirmation that the alternation between plate-like and columnar habits, and the re-emergence of columnar growth below −40 °C, arises from the strong temperature dependence of terrace step free energies and facet-specific attachment coefficients on basal and prism facets; (ii) refinement of classical habit diagrams through extended low-temperature measurements, yielding updated $\alpha(T)$ parameterizations that capture needle, bullet-rosette, and columnar regimes; (iii) quantitative laboratory reproduction of complex morphologies, including near-100% trigonal crystals via controlled surface perturbation; (iv) molecular-dynamics simulations, especially with machine-learned interatomic potentials, that have clarified the role of quasi-liquid layers (QLLs) in modulating step propagation barriers and facet-specific kinetics; and (v) multi-scale modeling frameworks that connect atomic-scale interfacial energetics to mesoscopic diffusion-limited growth and macroscopic branching instabilities, achieving quantitative agreement with laboratory data and in-situ observations.

Despite these advances, fundamental challenges remain. First, the quantitative influence of atmospheric impurities on growth kinetics is still poorly understood. Even trace concentrations of organic compounds, salts, and mineral dust can profoundly alter step energies, QLL stability, and facet-specific attachment coefficients, shifting habit-transition temperatures by several degrees Celsius. Yet the underlying molecular mechanisms and their parameterization for cloud and crystal-growth models remain largely unexplored. Second, existing $\alpha(T)$ parameterizations rely heavily on empirical fits rather than first-principles derivations from interfacial physics. This limits predictive capability for rare morphologies and extreme conditions in the upper troposphere or on icy planetary bodies. Third, fully predictive multi-scale modeling under realistic dynamic atmospheric conditions—incorporating three-dimensional ventilation effects, rapidly varying supersaturation, sedimentation-

https://doi.org/10.5194/egusphere-2026-3704
Preprint. Discussion started: 10 July 2026


induced reorientation, and aggregation—has not yet been achieved. Reconciliation of laboratory growth rates with in-situ observations is further limited by uncertainties in local supersaturation measurements.

Looking ahead, advances in high-resolution molecular-dynamics simulations, AI-assisted parameterization of interfacial kinetics, and next-generation in-situ imaging platforms—such as holographic microscopy and airborne probes—offer a clear path to address these challenges within the next decade. Snow crystals will continue to serve as a powerful natural laboratory for non-equilibrium interfacial pattern formation, where the interplay of diffusion, attachment kinetics, QLL dynamics, and instability amplification generates exceptional morphological diversity from a single crystalline phase. Resolving these questions will deepen our understanding of this paradigmatic system and advance general principles of non-equilibrium solidification relevant to atmospheric science, materials engineering, planetary cryoscience, and condensed matter physics.

## Data availability

No new data sets were generated in this review article. All underlying data are available from the original publications cited in the manuscript and listed in the references.

## Author contributions

L.Z.: Investigation, Writing – original draft. J.L.: Conceptualization, Supervision, Writing – review & editing. Y.H.: Conceptualization, Supervision, Writing – review & editing. All authors reviewed and approved the final manuscript.

## Competing interests

The authors declare that they have no conflict of interest.

## Disclaimer

The views expressed in this paper are those of the authors and do not necessarily reflect the views of the funding agencies or the publisher.

## Acknowledgements

The authors thank the Jiangsu Provincial Development and Reform Commission for funding the Polar and Extreme Environment Simulation Experiment Facility project.

https://doi.org/10.5194/egusphere-2026-3704
Preprint. Discussion started: 10 July 2026


**Financial support**

This research has been supported by the National Natural Science Foundation of China (grant no. 52506006) and the Jiangsu Provincial Development and Reform Commission through the Polar and Extreme Environment Simulation Experiment Facility project.

**References**

Abbatt, J. P. D.: Interactions of atmospheric trace gases with ice surfaces: adsorption and reaction, Chem. Rev., 103, 4783–4800, https://doi.org/10.1021/cr0206418, 2003.

Akhtar, S., Xu, M. H., Mohit, M., and Sasmito, A. P.: A comprehensive review of modeling water solidification for droplet freezing applications, Renew. Sustain. Energy Rev., 188, 113768, https://doi.org/10.1016/j.rser.2023.113768, 2023.

Bailey, M. and Hallett, J.: Growth rates and habits of ice crystals between −20 and −70 °C, J. Atmos. Sci., 61, 514–544, https://doi.org/10.1175/1520-0469(2004)061<0514:GRAHOI>2.0.CO;2, 2004.

Bailey, M. P. and Hallett, J.: A comprehensive habit diagram for atmospheric ice crystals: confirmation from the laboratory, AIRS II, and other field studies, J. Atmos. Sci., 66, 2888–2899, https://doi.org/10.1175/2009JAS2883.1, 2009.

Ball, P.: In retrospect: on the six-cornered snowflake, Nature, 480, 455, https://doi.org/10.1038/480455a, 2011.

Barnard, F. L.: Discovery of some initial sketches and notes for William Scoresby Junior's An Account of the Arctic Regions, Polar Rec., 60, e13, https://doi.org/10.1017/S0032247424000056, 2024.

Barrett, J. W., Garcke, H., and Nürnberg, R.: Numerical computations of faceted pattern formation in snow crystal growth, Phys. Rev. E, 86, 011604, https://doi.org/10.1103/PhysRevE.86.011604, 2012.

Bartels-Rausch, T., Jacobi, H.-W., Kahan, T. F., Thomas, J. L., Thomson, E. S., Abbatt, J. P. D., Ammann, M., Blackford, J. R., Bluhm, H., Boxe, C., Domine, F., Frey, M. M., Gladich, I., Guzmán, M. I., Heger, D., Huthwelker, T., Klán, P., Kuhs, W. F., Kuo, M. H., Maus, S., Moussa, S. G., McNeill, V. F., Newberg, J. T., Pettersson, J. B. C., Roeselová, M., and Sodeau, J. R.: A review of air–ice chemical and physical interactions (AICI): liquids, quasi-liquids, and solids in snow, Atmos. Chem. Phys., 14, 1587–1633, https://doi.org/10.5194/acp-14-1587-2014, 2014.

Bartlett, J., Van den Heuvel, A. P., and Mason, B. J.: The growth of ice crystals in an electric field, Z. Angew. Math. Phys., 14, 599–610, https://doi.org/10.1007/BF01601363, 1963.

Bentley, W. A. and Humphreys, W. J.: Snow Crystals, McGraw-Hill Book Company, New York, 1931.

Bluhm, H., Ogletree, D. F., Fadley, C. S., Hussain, Z., and Salmeron, M.: The premelting of ice studied with photoelectron spectroscopy, J. Phys.: Condens. Matter, 14, L227–L233, https://doi.org/10.1088/0953-8984/14/8/108, 2002.

Cao, L., Jones, A. K., Sikka, V. K., Wu, J., and Gao, D.: Anti-icing superhydrophobic coatings, Langmuir, 25, 12444–12448, https://doi.org/10.1021/la902882b, 2009.

https://doi.org/10.5194/egusphere-2026-3704
Preprint. Discussion started: 10 July 2026


Chu, F. Q., Hu, Z. F., Feng, Y. H., Lai, N. C., Wu, X. M., and Wang, R. Z.: Advanced anti-icing strategies and technologies by macrostructured photothermal storage superhydrophobic surfaces, Adv. Mater., 36, 2401234, https://doi.org/10.1002/adma.202401234, 2024.

Cui, B., Xu, P. Z., Li, X. Z., Fan, K. L., Guo, X., and Tong, L.: Low-dimensional and confined ice, Annu. Rev. Mater. Res., 53, 371–397, https://doi.org/10.1146/annurev-matsci-080921-101732, 2023.

Curiotto, S., Paulovics, D., Raufaste, C., Celestini, F., Frisch, T., Leroy, F., Cheynis, F., and Müller, P.: Atomistic description of interdroplet ice-bridge formation during condensation frosting, Langmuir, 39, 579–587, https://doi.org/10.1021/acs.langmuir.2c02835, 2023.

D'Acunzi, M., Sharifi-Aghili, A., Hegner, K. I., and Vollmer, D.: Super liquid repellent coatings against the everyday life wear: heating, freezing, scratching, iScience, 24, 102428, https://doi.org/10.1016/j.isci.2021.102428, 2021.

Dai, X., Yuan, Y., Xiang, H., Wei, L., Hong, C., Xiao, J., Zhao, Y., Yang, T., and Liao, R.: A composite nanoporous superhydrophobic film with anti-icing properties and durability: from laboratory test to field validation, Colloids Surf. A, 728, 138480, https://doi.org/10.1016/j.colsurfa.2025.138480, 2026.

Demange, G., Patte, R., Zapolsky, H., and Brunel, M.: A phase field model for snow crystal growth in three dimensions, npj Comput. Mater., 3, 15, https://doi.org/10.1038/s41524-017-0018-7, 2017.

Dosch, H., Lied, A., and Bilgram, J. H.: Glancing-angle X-ray scattering studies of the premelting of ice surfaces, Surf. Sci., 327, 145–164, https://doi.org/10.1016/0039-6028(94)00801-9, 1995.

Elbaum, M., Lipson, S. G., and Dash, J. G.: Optical study of surface melting on ice, J. Cryst. Growth, 129, 491–505, https://doi.org/10.1016/0022-0248(93)90479-H, 1993.

Feistel, R. and Wagner, W.: Sublimation pressure and sublimation enthalpy of H2O ice Ih between 0 and 273.16 K, Geochim. Cosmochim. Acta, 71, 36–45, https://doi.org/10.1016/j.gca.2006.08.034, 2007.

Gerber, D., Wilen, L. A., Poydenot, F., Dufresne, E. R., and Style, R. W.: Stress accumulation by confined ice in a temperature gradient, Proc. Natl. Acad. Sci. USA, 119, e2203663119, https://doi.org/10.1073/pnas.2203663119, 2022.

Harrington, J. Y. and Pokrifka, G. F.: Approximate models for lateral growth on ice crystal surfaces during vapor depositional growth, J. Atmos. Sci., 78, 967–981, https://doi.org/10.1175/JAS-D-20-0221.1, 2021.

Hauer, L., Wong, W. S. Y., Sharifi-Aghili, A., Kondic, L., and Vollmer, D.: Frost spreading and pattern formation on microstructured surfaces, Phys. Rev. E, 104, 044901, https://doi.org/10.1103/PhysRevE.104.044901, 2021.

Hidas, K., Tommasi, A., Mainprice, D., Chauve, T., Barou, F., and Montagnat, M.: Microstructural evolution during thermal annealing of ice-I, J. Struct. Geol., 99, 31–44, https://doi.org/10.1016/j.jsg.2017.04.007, 2017.

Hoffmann, F.: Effects of entrainment and mixing on the Wegener–Bergeron–Findeisen process, J. Atmos. Sci., 77, 2279–2296, https://doi.org/10.1175/JAS-D-19-0289.1, 2020.

Hong, J., Tian, Y., Liang, T., Liu, X., Song, Y., Guan, D., Yan, Z., Guo, J., Tang, B., Cao, D., Guo, J., Chen, J., Pan, D., Xu, L. M., Wang, E. G., and Jiang, Y.: Imaging surface structure and premelting of ice Ih with atomic resolution, Nature, 630, 375–380, https://doi.org/10.1038/s41586-024-07427-8, 2024.

https://doi.org/10.5194/egusphere-2026-3704
Preprint. Discussion started: 10 July 2026


Huang, S., Hu, W., Chen, J., Wu, Z., and Fu, P.: Overview of biological ice nucleating particles in the atmosphere, Environ. Int., 146, 106197, https://doi.org/10.1016/j.envint.2020.106197, 2021.

Huang, W., Huang, J., Guo, Z., and Liu, W.: Icephobic/anti-icing properties of superhydrophobic surfaces, Adv. Colloid Interface Sci., 304, 102658, https://doi.org/10.1016/j.cis.2022.102658, 2022.

Kärcher, B.: Process-based simulation of aerosol–cloud interactions in a one-dimensional cirrus model, J. Geophys. Res.-Atmos., 125, e2019JD031847, https://doi.org/10.1029/2019JD031847, 2020.

Kärcher, B. and Basko, M. M.: Trapping of trace gases in growing ice crystals, J. Geophys. Res.-Atmos., 109, D22204, https://doi.org/10.1029/2004JD005151, 2004.

Kikuchi, K., Kameda, T., Higuchi, K., and Yamashita, A.: A global classification of snow crystals, ice crystals, and solid precipitation based on observations from middle latitudes to polar regions, Atmos. Res., 132, 460–472, https://doi.org/10.1016/j.atmosres.2013.06.006, 2013.

Kling, T., Kling, F., and Donadio, D.: Structure and dynamics of the quasi-liquid layer at the surface of ice from molecular simulations, J. Phys. Chem. C, 122, 24780–24787, https://doi.org/10.1021/acs.jpcc.8b07724, 2018.

Kuhs, W. F., Sippel, C., Falenty, A., and Hansen, T. C.: Extent and relevance of stacking disorder in “ice Ic”, Proc. Natl. Acad. Sci. USA, 109, 21259–21264, https://doi.org/10.1073/pnas.1210331110, 2012.

Kuroda, T. and Lacmann, R.: Growth kinetics of ice from the vapor phase and its growth forms, J. Cryst. Growth, 56, 189–205, https://doi.org/10.1016/0022-0248(82)90028-8, 1982.

Lamb, K. D., Harrington, J. Y., Clouser, B. W., Moyer, E. J., Sarkozy, L., Ebert, V., Möhler, O., and Saathoff, H.: Re-evaluating cloud chamber constraints on depositional ice growth in cirrus clouds – Part 1: model description and sensitivity tests, Atmos. Chem. Phys., 23, 6043–6064, https://doi.org/10.5194/acp-23-6043-2023, 2023.

Langer, J. S.: Instabilities and pattern formation in crystal growth, Rev. Mod. Phys., 52, 1–28, https://doi.org/10.1103/RevModPhys.52.1, 1980.

Libbrecht, K. G.: The physics of snow crystals, Rep. Prog. Phys., 68, 855–895, https://doi.org/10.1088/0034-4885/68/4/R03, 2005.

Libbrecht, K. G.: An improved apparatus for measuring the growth of ice crystals from water vapor, arXiv [preprint], https://doi.org/10.48550/arXiv.1109.1511, 2011a.

Libbrecht, K. G.: Observations of an edge-enhancing instability in snow crystal growth near −15 °C, arXiv [preprint], https://doi.org/10.48550/arXiv.1111.2786, 2011b.

Libbrecht, K. G.: Toward a comprehensive model of snow crystal growth dynamics: 1. Overarching features and physical origins, arXiv [preprint], https://doi.org/10.48550/arXiv.1211.5555, 2012a.

Libbrecht, K. G.: An edge-enhancing crystal growth instability caused by structure-dependent attachment kinetics, arXiv [preprint], https://doi.org/10.48550/arXiv.1209.4932, 2012b.

Libbrecht, K. G.: Toward a comprehensive model of snow crystal growth dynamics: 2. Structure-dependent attachment kinetics near −5 °C, arXiv [preprint], https://doi.org/10.48550/arXiv.1302.1231, 2013.

https://doi.org/10.5194/egusphere-2026-3704
Preprint. Discussion started: 10 July 2026


Libbrecht, K. G.: Measurements of cylindrical ice crystal growth limited by combined particle and heat diffusion, arXiv [preprint], https://doi.org/10.48550/arXiv.1602.02683, 2016.

Libbrecht, K. G.: Physical dynamics of ice crystal growth, Annu. Rev. Mater. Res., 47, 271–295, https://doi.org/10.1146/annurev-matsci-070616-124135, 2017.

Libbrecht, K. G.: A quantitative physical model of the snow crystal morphology diagram, arXiv [preprint], https://doi.org/10.48550/arXiv.1910.09067, 2019a.

Libbrecht, K. G.: A versatile apparatus for measuring the growth rates of small ice prisms from the vapor phase, arXiv [preprint], https://doi.org/10.48550/arXiv.1912.09440, 2019b.

Libbrecht, K. G.: Toward a comprehensive model of snow crystal growth: 6. Ice attachment kinetics near −5 °C, arXiv [preprint], https://doi.org/10.48550/arXiv.1912.03230, 2019c.

Libbrecht, K. G.: Triangular snowflakes: growing structures with three-fold symmetry using a hexagonal ice crystal lattice, arXiv [preprint], https://doi.org/10.48550/arXiv.2106.09809, 2021a.

Libbrecht, K. G.: A taxonomy of snow crystal growth behaviors: 1. Using c-axis ice needles as seed crystals, arXiv [preprint], https://doi.org/10.48550/arXiv.2109.00098, 2021b.

Libbrecht, K. G.: Snow Crystals, Princeton University Press, Princeton, ISBN 978-0-691-20037-8, 2022.

Libbrecht, K. G.: A taxonomy of snow crystal growth behaviors: 2. Quantifying the Nakaya diagram, arXiv [preprint], https://doi.org/10.48550/arXiv.2306.13087, 2023.

Libbrecht, K. G. and Arnold, H. M.: Measurements of ice crystal growth rates in air at −5 and −10 °C, arXiv [preprint], https://doi.org/10.48550/arXiv.0912.2518, 2009a.

Libbrecht, K. G. and Arnold, H. M.: Aerodynamic stability and the growth of triangular snow crystals, Microscope, 57, 77–84, 2009b.

Libbrecht, K. G. and Morrison, H. C.: A convection chamber for measuring ice crystal growth dynamics, arXiv [preprint], https://doi.org/10.48550/arXiv.0809.4869, 2008.

Libbrecht, K. G. and Rickerby, M. E.: Measurements of surface attachment kinetics for faceted ice crystal growth, J. Cryst. Growth, 377, 1–8, https://doi.org/10.1016/j.jcrysgro.2013.04.037, 2013.

Libbrecht, K. G. and Tanusheva, V. M.: Electrically induced morphological instabilities in free dendrite growth, Phys. Rev. Lett., 81, 176–179, https://doi.org/10.1103/PhysRevLett.81.176, 1998.

Libbrecht, K. G. and Walkling, J.: A comprehensive model of snow crystal faceting, arXiv [preprint], https://doi.org/10.48550/arXiv.2306.04042, 2023.

Libbrecht, K. G., Crosby, T., and Swanson, M.: Electrically enhanced free dendrite growth in polar and non-polar systems, J. Cryst. Growth, 240, 241–254, https://doi.org/10.1016/S0022-0248(02)00861-8, 2002.

Llombart, P., Noya, E. G., and MacDowell, L. G.: Surface phase transitions and crystal habits of ice in the atmosphere, Sci. Adv., 6, eaay9322, https://doi.org/10.1126/sciadv.aay9322, 2020.

https://doi.org/10.5194/egusphere-2026-3704
Preprint. Discussion started: 10 July 2026


Lupi, L., Hudait, A., Peters, B., Grünwald, M., Mullen, R. G., Nguyen, A. H., and Molinero, V.: Role of stacking disorder in ice nucleation, Nature, 551, 218–222, https://doi.org/10.1038/nature24279, 2017.

MacDowell, L. G.: The key physics of ice premelting, J. Chem. Phys., 164, 030901, https://doi.org/10.1063/5.0302303, 2026.

Magono, C. and Lee, C. W.: Meteorological classification of natural snow crystals, J. Fac. Sci. Hokkaido Univ., Ser. VII, 2, 321–335, 1966.

Maurais, J., Wespiser, C., Robidas, R., Legault, C. Y., and Ayotte, P.: Trapping intermediates of the NO2 hydrolysis reaction on ice, Faraday Discuss., 258, 546–567, https://doi.org/10.1039/d4fd00161c, 2025.

McMurdie, L. A., Heymsfield, G. M., Yorks, J. E., Braun, S. A., Skofronick-Jackson, G., Rauber, R. M., Yuter, S., Colle, B., McFarquhar, G. M., Poellot, M., Novak, D. R., Lang, T. J., Kroodsma, R., McLinden, M., Oue, M., Kollias, P., Kumjian, M. R., Greybush, S. J., Heymsfield, A. J., Finlon, J. A., McDonald, V. L., and Nicholls, S.: Chasing snowstorms: the Investigation of Microphysics and Precipitation for Atlantic Coast-Threatening Snowstorms (IMPACTS) campaign, Bull. Amer. Meteorol. Soc., 103, E1243–E1269, https://doi.org/10.1175/BAMS-D-20-0246.1, 2022.

Mitsui, T. and Aoki, K.: Fluctuation spectroscopy of surface melting of ice with and without impurities, Phys. Rev. E, 99, 012801, https://doi.org/10.1103/PhysRevE.99.012801, 2019.

Mochizuki, K. and Molinero, V.: Antifreeze glycoproteins bind reversibly to ice via hydrophobic groups, J. Am. Chem. Soc., 140, 4803–4811, https://doi.org/10.1021/jacs.7b13672, 2018.

Mochizuki, K., Murata, K., and Zhang, X.: Microscopic ordering of supercooled water on the ice basal face, Commun. Mater., 4, 33, https://doi.org/10.1038/s43246-023-00359-2, 2023.

Mohammadian, B., Namdari, N., Yassine, A. H. A., Heil, J., and Sojoudi, H.: Interfacial phenomena in snow from its formation to accumulation and shedding, Adv. Colloid Interface Sci., 294, 102480, https://doi.org/10.1016/j.cis.2021.102480, 2021.

Morrison, H., van Lier-Walqui, M., Fridlind, A. M., Grabowski, W. W., Harrington, J. Y., Hoose, C., Korolev, A., Kumjian, M. R., Milbrandt, J. A., Pawlowska, H., Posselt, D. J., Prat, O. P., Reimel, K. J., Shima, S.-I., van Diedenhoven, B., and Xue, L.: Confronting the challenge of modeling cloud and precipitation microphysics, J. Adv. Model. Earth Syst., 12, e2019MS001689, https://doi.org/10.1029/2019MS001689, 2020.

Murray, B. J., O'Sullivan, D., Atkinson, J. D., and Webb, M. E.: Ice nucleation by particles immersed in supercooled cloud droplets, Chem. Soc. Rev., 41, 6519–6554, https://doi.org/10.1039/C2CS35200A, 2012.

Murray, B. J., Salzmann, C. G., Heymsfield, A. J., Dobbie, S., Neely, R. R., and Cox, C. J.: Trigonal ice crystals in Earth's atmosphere, Bull. Amer. Meteorol. Soc., 96, 1685–1696, https://doi.org/10.1175/BAMS-D-13-00122.1, 2015.

Murphy, D. M. and Koop, T.: Review of the vapour pressures of ice and supercooled water for atmospheric applications, Q. J. Roy. Meteor. Soc., 131, 1539–1565, https://doi.org/10.1256/qj.04.94, 2005.

Nagata, Y., Hama, T., Backus, E. H. G., Mezger, M., Bonn, D., Bonn, M., and Sazaki, G.: The surface of ice under equilibrium and nonequilibrium conditions, Acc. Chem. Res., 52, 1006–1015, https://doi.org/10.1021/acs.accounts.8b00615, 2019.

https://doi.org/10.5194/egusphere-2026-3704
Preprint. Discussion started: 10 July 2026


Nakaya, U.: Snow Crystals: Natural and Artificial, Harvard University Press, Cambridge, MA, 1954.

Needham, J. and Lu, G. D.: Science and Civilisation in China: Volume 3, Mathematics and the Sciences of the Heavens and the Earth, Cambridge University Press, Cambridge, 1959.

Pal, D., Hall, R., Nazarenko, Y., Barrie, L., and Ariya, P. A.: Microphysical detection of nano-ice nuclei to ice crystals: a platform for ice nucleation research, npj Clim. Atmos. Sci., 8, 204, https://doi.org/10.1038/s41612-025- 01062-4, 2025.

Pedersen, A., Wikfeldt, K. T., Karssemeijer, L., Cuppen, H., and Jónsson, H.: Molecular reordering processes on ice (0001) surfaces from long timescale simulations, J. Chem. Phys., 141, 234706, https://doi.org/10.1063/1.4903812, 2014.

Petrenko, V. and Whitworth, R.: Physics of Ice, Oxford University Press, Oxford, 1999.

Ping, Y.: Descartes and the Meteorology, Advances in Meteorological Science and Technology, 6(1): 46-49. DOI: 10.3969/j.issn.2095-1973.2016.01.008, 2016.

Porco, C. C., Helfenstein, P., Thomas, P. C., Ingersoll, A. P., Wisdom, J., West, R., Neukum, G., Denk, T., Wagner, R., and Roatsch, T.: Cassini observes the active south pole of Enceladus, Science, 311, 1393–1401, https://doi.org/10.1126/science.1123013, 2006.

Postberg, F., Khawaja, N., Abel, B., Choblet, G., Glein, C. R., Gudipati, M. S., Henderson, B. L., Hsu, H. W., Kempf, S., Klenner, F., Moragas-Klostermeyer, G., Magee, B., Nölle, L., Perry, M., Reviol, R., Schmidt, J., Srama, R., Stolz, F., Tobie, G., Trieloff, M., and Waite, J. H.: Macromolecular organic compounds from the depths of Enceladus, Nature, 558, 564–568, https://doi.org/10.1038/s41586-018-0246-4, 2018.

Pruppacher, H. R. and Klett, J. D.: Microphysics of Clouds and Precipitation, Springer, Dordrecht, 2010.

Rapp, C. N., Niu, S., Armstrong, N. C., Shen, X., Berkemeier, T., Surratt, J. D., Zhang, Y., and Cziczo, D. J.: Ice-nucleating properties of glassy organic and organosulfate aerosol, Atmos. Chem. Phys., 25, 5519–5536, https://doi.org/10.5194/acp-25-5519-2025, 2025.

Roth, L., Saur, J., Retherford, K. D., Strobel, D. F., Feldman, P. D., McGrath, M. A., and Nimmo, F.: Transient water vapor at Europa's south pole, Science, 343, 171–174, https://doi.org/10.1126/science.1247051, 2014.

Sadtchenko, V. and Ewing, G. E.: Interfacial melting of thin ice films: an infrared study, J. Chem. Phys., 116, 4686–4697, https://doi.org/10.1063/1.1449947, 2002.

Schlesinger, D., Lowe, S. J., Olenius, T., Kong, X. R., Pettersson, J. B. C., and Riipinen, I.: Molecular perspective on water vapor accommodation into ice and its dependence on temperature, J. Phys. Chem. A, 124, 10879–10889, https://doi.org/10.1021/acs.jpca.0c09357, 2020.

Seinfeld, J. H. and Pandis, S. N.: Atmospheric Chemistry and Physics: From Air Pollution to Climate Change, 3rd edn., John Wiley & Sons, Hoboken, NJ, 2016.

Shi, J. H., Fulford, M., Salvalaglio, M., and Molteni, C.: Unveiling the face-dependent ice growth kinetics: insights from molecular dynamics on the basal and prism surfaces, J. Chem. Phys., 162, 054714, https://doi.org/10.1063/5.0240795, 2025.

Shimada, W., Yoshii, T., Mochizuki, A., and Ohtake, K.: Three-dimensional aspects of sidebranch formation during the growth of snow crystals, J. Cryst. Growth, 548, 125812, https://doi.org/10.1016/j.jcrysgro.2020.125812, 2020.

https://doi.org/10.5194/egusphere-2026-3704
Preprint. Discussion started: 10 July 2026


Sibley, D. N., Llombart, P., Noya, E. G., Archer, A. J., and MacDowell, L. G.: How ice grows from premelting films and water droplets, Nat. Commun., 12, 239, https://doi.org/10.1038/s41467-020-20318-6, 2021.

Sosso, G. C., Chen, J., Cox, S. J., Fitzner, M., Pedevilla, P., Zen, A., and Michaelides, A.: Crystal nucleation in liquids: open questions and future challenges in molecular dynamics simulations, Chem. Rev., 116, 7078–7116, https://doi.org/10.1021/acs.chemrev.5b00744, 2016.

Stoll, N., Eichler, J., Hörhold, M., Shigeyama, W., and Weikusat, I.: A review of the microstructural location of impurities in polar ice and their impacts on deformation, Front. Earth Sci., 8, 615613, https://doi.org/10.3389/feart.2020.615613, 2021.

Vázquez-Martín, S., Kuhn, T., and Eliasson, S.: Shape dependence of snow crystal fall speed, Atmos. Chem. Phys., 21, 7545–7565, https://doi.org/10.5194/acp-21-7545-2021, 2021.

Xu, W. Y.: Collected Annotations on Han Shi Wai Zhuan, Zhonghua Book Company, Beijing, 2009.

Yasuda, I., Endo, K., Arai, N., and Yasuoka, K.: In-layer inhomogeneity of molecular dynamics in quasi-liquid layers of ice, Commun. Chem., 7, 117, https://doi.org/10.1038/s42004-024-01197-0, 2024.

Yettapu, G. R., Manning, L. B., and Cyran, J. D.: Elucidating how trace gases interact with ice surfaces utilizing sum frequency generation spectroscopy, Faraday Discuss., 258, 521–531, https://doi.org/10.1039/d4fd00157e, 2025.

Yokoyama, E., Yoshizaki, I., Shimaoka, T., Sone, T., Kiyota, T., and Furukawa, Y.: Measurements of growth rates of an ice crystal from supercooled heavy water under microgravity conditions: basal face growth rate and tip velocity of a dendrite, J. Phys. Chem. B, 115, 8739–8745, https://doi.org/10.1021/jp110634t, 2011.

Zhang, R. Y., Khalizov, A., Wang, L., Hu, M., and Xu, W.: Nucleation and growth of nanoparticles in the atmosphere, Chem. Rev., 112, 1957–2011, https://doi.org/10.1021/cr2001756, 2012.